The Pennsylvania State University

The Graduate School

DEVELOPMENT OF A HIGH-DENSITY INITIATION MECHANISM FOR SUPERCRITICAL NITROMETHANE DECOMPOSITION

A Thesis in

Mechanical Engineering

by

Christopher N. Burke

Submitted in Partial Fulfillment
of the Requirements
for the Degree of

Master of Science

August 2020

The thesis of Christopher N. Burke was reviewed and approved by the following:

Richard A. Yetter
Professor of Mechanical Engineering
Thesis Co-Advisor

Adrianus C. van Duin
Professor of Mechanical Engineering
Thesis Co-Advisor

Jacqueline A. O'Connor
Professor of Mechanical Engineering

Karen Thole
Professor of Mechanical Engineering
Mechanical Engineering Department Head

Abstract:

This thesis outlines the bottom-up development of a high pressure, high-density initiation mechanism for nitromethane decomposition. Using reactive molecular dynamics (ReaxFF), a hydrogen-abstraction initiation mechanism for nitromethane decomposition that occurs at initial supercritical densities of 0.83 grams per cubic centimeter was investigated and a mechanism was constructed as an addendum for existing mechanisms. The reactions in this mechanism were examined and the pathways leading from the new initiation set into existing mechanism are discussed, with ab-initio/DFT level data to support them, as well as a survey of other combustion mechanisms containing analogous reactions. C_2 carbon chemistry and soot formation pathways were also included to develop a complete high-pressure mechanism to compare to the experimental results of Derk. C_2 chemistry, soot chemistry, and the hydrogen-abstraction initiation mechanism were appended to the baseline mechanism used by Boyer and analyzed in Chemkin as a temporal, ideal gas decomposition. The analysis of these results includes a comprehensive discussion of the observed chemistry and the implications thereof.

Table of Contents

List of Figures

List of Tables

Acknowledgements

I would like to thank everyone that helped me get to the point in both my career and my education that I am currently at. Richard Yetter, Adri van Duin, and Eric Boyer have all been excellent mentors to me during the duration of my MS. My coworkers have been excellent in helping me accomplish my degree; in helping answer my questions and in being patient with me while I work through my thesis and coursework. My work mentor, Ray Roberts, has also been excellent in helping me with my work by sharpening my critical thinking and my aiding in reading and reviewing my work. Lastly, my fellow student, room-mate, and friend Gerardo Talamantes has been unparalleled to me during my time at Penn State. His support over the past few years has been nothing short of invaluable and critical in making this rewarding journey become a reality.

Dedications

I would like to dedicate this thesis to my parents, Paul and Janice Burke. Their support during my work has been no different than it has ever been throughout my life- unconditional.

CHAPTER ONE

Introduction

This thesis defines a finite-rate chemical kinetic mechanism for the high-density combustion of supercritical nitromethane. The kinetic mechanism was developed as an addendum to currently accepted and well proven mechanisms[1][2] for liquid, gaseous, and critical nitromethane, defining a potential change in the core initiation chemistry as both a fuel and monopropellant. The mechanism aims to improve the calculations of flame structure, flame temperature, and ignition delay times at high supercritical densities. Combustion of nitromethane has been extensively studied as both a fuel and a monopropellant for use in automobiles, rockets, ballistic projectiles, and various other applications. A polar energetic nitro compound such as nitromethane has a wide range of applications because it can be utilized as a propellant without the need for an oxidizer, effectively maximizing specific energy and energy density on a system level.

1.1 Applications of Nitromethane

Nitromethane is often used in high performance racing applications. Top Fuel racing brackets in the National Hot Rod Association (NHRA) utilize nitromethane as their fuel source in air-breathing supercharged engines.[3] Raviteja, Ramakrishna, and Ramesh showed that the addition of nitromethane to gasoline increased the laminar flame speed across a range of equivalence ratios from 0.6 to 1.6 by indicating a higher peak pressure with increasing nitromethane

content, implying that the laminar flame speed of pure nitromethane is higher than that of typical petrol with air.[4] This makes nitromethane a better suited fuel for high revving engines; particularly those with high piston speeds. The dwell time of a piston at top dead center, the time during which the system is at a nearly constant volume, is very short; on the order of one millisecond at 7,000 revolutions per minute.[5] The faster burn rate that nitromethane provides is required in order to complete the combustion process in sufficient time such that the thermodynamic cycle still resembles that of an Otto cycle, with either constant-volume or limited-pressure heat addition. Power output would otherwise suffer remarkably, as the rapid expansion of the downward moving piston would extinguish a slower burning flame. Even within lower engine speeds attainable with petrol fuel, power increase can be realized through ignition timing adjustments; an ignition event that occurs later in the compression stroke minimizes the pumping losses associated with the compression of hot combustion products as they form.

The lower heating value of nitromethane is marginally more than 25% that of petrol gasoline, being 44.0 MJ/kg (18.9 kBTU/lb_m) for gasoline[5] and 11.3 MJ/kg (4.9 kBTU/lb_m) for nitromethane[6]. Based on stoichiometric ratios for the complete aerobic combustion of both fuels, nitromethane requires 13% less air by mass. Accounting for this in the calorific content of the fuel, nitromethane is conclusively a more suitable fuel for high speed racing applications; the total specific energy of the fuel and oxidizer mixture is approximately 2.25 times higher than that of gasoline. Finally, the adiabatic flame temperature of

nitromethane is higher than petrol gasoline, as calculated from a gas-phase reference state.[7] The latent heat of vaporization is higher as well, offsetting the thermal effect and maintaining a lower temperature of engine operation.[8],[9] For all these reasons, nitromethane has found itself applied in the sub-scaled model aviation community, as well as in high performance racing. The increased energy density and power capability is vastly important in model-scale aviation, where volume and mass limitations greatly drive the design of the craft, with cost following closely behind given that the majority of the community is composed of hobbyists.

Air independent propulsion (AIP) has important application in many different facets of engineering technology. Rocketry, undersea engines, and liquid gun propellants are three large areas of interest for this technical application.[10][11][12][13][14] Rockets are often depended upon to operate in environments with very low useable oxygen, and by definition, undersea vehicles are expected to always operate without air. Due to this, propulsion needs to be generated through means alternative to aerobic combustion.[10] Onboard oxidizer storage is a potential alternative, but generally avoided unless additional power requirements necessitate the use of an oxidizer. The additional balance of plant required to store and supply this oxidant consumes space and mass, which are valuable in rocket and undersea vehicle systems, without contributing significantly to range capability (assuming the oxidant does not supply energy by itself, such as hydrogen peroxide). Battery technologies can be used as well, but are ineffective in generating thrust in rocket engines and, due to the high density

of their components, lead to a system that may have appropriate volumetric energy density, but low specific energy.[15] Monopropellant fuels provide an excellent compromise, supplying comparable energy density and a high specific energy to compliment. Monopropellant-based propulsion systems require only enough balance of plant to store and use the fuel, leading to minimal amounts of lost space and weight.[10]

Liquid monopropellants were also applied to the field of gun propellants as well as missiles and undersea vehicles.[12] In typical artillery and other ballistic projectile weaponry, a solid propellant is relied upon to rapidly decompose into gaseous products, generating pressure and impulse to propel the projectile. Solid propellants require the design of solid grains to tailor burn rate, which is an important factor controlling the pressure curve and evening out the impulse applied to the projectile.[13] An even impulse and consistent pressure are key components of repeatable and precise internal ballistics. Liquid propellants are desirable for this reason because they can be fed and metered into the system, yielding more control over the entire combustion process.[12] This technology was studied for nearly forty years after the Second World War, and included studies of monopropellants such as hydrazine, nitromethane, and Otto fuel II.

1.2 Monopropellants and Decomposition Chemistry

Monopropellants have been used for over a century with application in rocketry, jet engines, and undersea propulsion. Historically, hydrogen peroxide was used for these purposes, decomposing into steam, oxygen, and heat, with notable applications such as the American Redstone and German V2 rockets.[11]

Hydrogen peroxide-based propulsion was being used in the torpedo community around this time as well, as energy and power density requirements forced engineers to move away from flywheel energy storage and compressed air turbines.[14] Nitromethane grew in popularity during the early era in rocket propulsion, but was at a lower technical readiness level than hydrogen peroxide as a propellant source, and was ultimately displaced by the more energy-dense hydrazine by the 1940's.[11] Hydrogen peroxide, nitromethane, and hydrazine fuels are representative of the full spectrum of chemistry. These hydrocarbon species, excluding hydrogen peroxide, contain either oxygen-bearing nitrate/nitro functional groups, or the more chemically basic amine groups. Some more modern monopropellants and explosives contain both functional groups, known as nitramines. Specific compounds, such as RDX and HMX, have been very popular since World War II and others, such as Ammonium Dinitramide (ADN) have been discovered and investigated much more recently.[16][17]

Monopropellants such as ethyl nitrate, isopropyl nitrate, and propylene glycol dinitrate, like nitromethane, utilize oxygen atoms in their nitrogen based functional groups to oxidize the base hydrocarbon and release the energy held within. These reactions can be tailored to proceed very rapidly with proper synthesis and design by placing reacting functional groups within close proximity on the same molecule and verifying that they are at the thermodynamically favorable active sites. Conversely, their rates can be hindered by utilizing steric strain in design of the molecule to keep these functional groups away from each other, or by utilizing sites that are less thermodynamically preferable for reaction,

thus delaying the onset of decomposition and heat release. Burning rates are also hampered by the use of a stabilizer, such as dibutyl or dioctyl sebacate, that absorb thermal energy from the propellant over the course of the reaction and retard thermal runaway.[18]

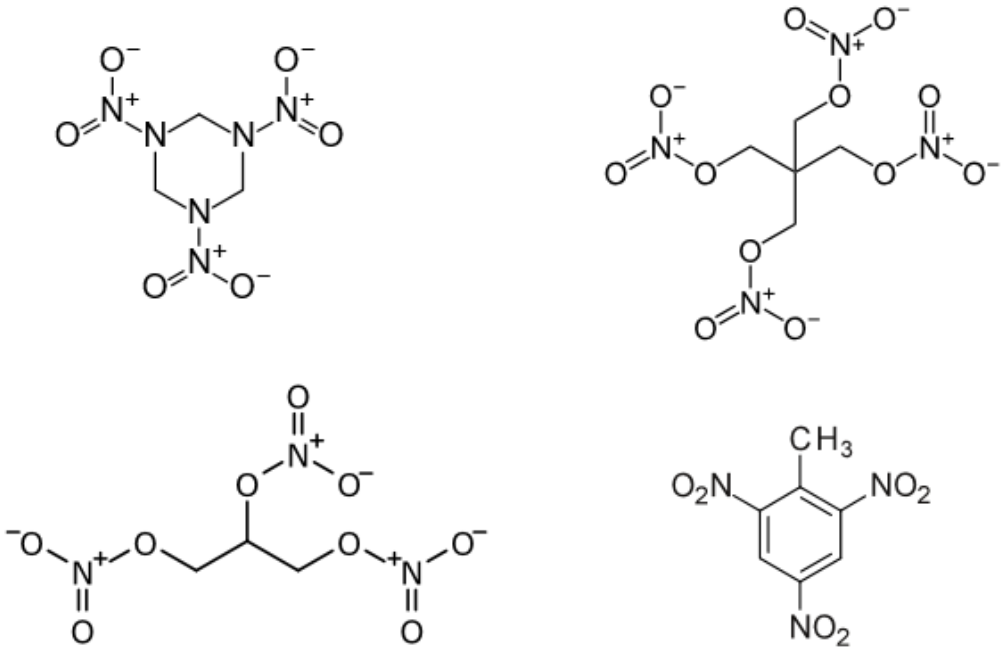

Figure One: Chemical Structure of Common Nitro/Nitrate Explosives and Monopropellants

Much common monopropellant chemistry involves the use of nitro or nitrate functional groups in their chemical structure. Exceptions to this rule do exist, such as hydrazine, or those developed in recent history such as triacetone triperoxide (TATP). TATP was specifically developed as a high energy explosive for use in improvised devices that remain undetectable by modern sensors that are tailored to look for nitrogen-based chemicals.[19]

Covalently bonded nitro groups and nitrate esters provide an oxygen source of improved thermal stability in comparison to other oxidizer groups, which tend to be ionic in nature such as perchlorates and permanganates.[20][21] Nitro-functionalized compounds and nitrate esters also promote high heat release with the formation of N_2 as a product, an elemental diatomic species with one of the

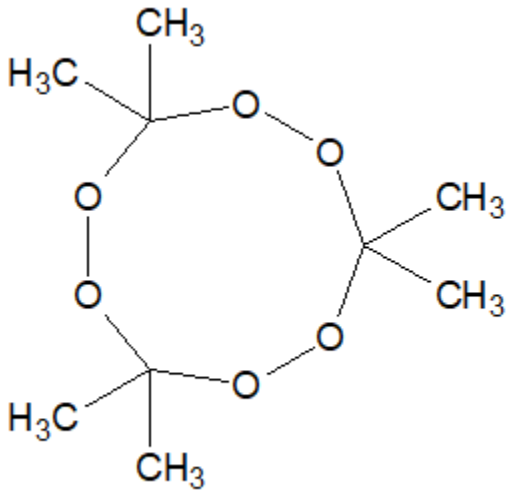

Figure Two: Chemical Structure of Triacetone Triperoxide (TATP)

most thermally stable chemical bonds known to exist.[22] Hydrocarbon monopropellants have a tendency to be fuel rich due to the difficulty of storing a stoichiometric amount of oxygen in the structure of the propellant. As a result, they form a reducing environment and the chemistry acts according to such. Engine components can be made out of less expensive materials since they only need to maintain integrity under thermal load without the concern of chemical stability against a strongly oxidizing environment, which becomes an issue with engines that use oxidizers or inorganic monopropellants such as nitric acid, hydroxylammonium nitrate, or hydroxylammonium perchlorate.[20][23] The

converse is that the fuel rich burning leads to a high sooting tendency of these fuels, particularly those with dominant C_2, C_3, or higher order carbon chemistry.

1.3 Research Objectives

The objective of this research is to increase our understanding of the supercritical nitromethane flame behavior by delving into the chemistry using a bottom-up approach. Monopropellant decomposition is complex and nitromethane, being of simple chemical structure, offers insight into these complex mechanisms. Figure three shows that the flame speed of nitromethane follows three basic regimes as a function of pressure.[24] The first regime is the slowest burning, occurring between 3.6 and 18.2 megapascal pressure (522 to 2640 psi). This is the sub-critical burning regime, where nitromethane liquid burns and the evaporation of liquid nitromethane into the gas phase has a strong effect on the flame speed. The next regime occurs between 18.2 and 40.8 megapascal (2640 to 5918 psi). This is the first stage of accelerated supercritical burning, where combustion-induced turbulence is abundantly present. In this stage, the flame is transitioning between being limited by the evaporation rate of the liquid interface and the chemistry of the gas-phase flame itself. The last regime occurs above 40.8 megapascal pressure (5918 psi), where the slope of flame speed as a logarithmic function of pressure is nearly the same as it was in the first regime, with a higher intercept. This work was performed by Boyer and, later, Derk in the High-Pressure Combustion Laboratory (HPCL) at the Pennsylvania State University.[24][1] The burn rates for these three pressure regimes are given by Derk as follows.

$$r_b(^{mm}/_s) = 0.183[P(MPa)]^{1.15} \; for \; 3.6 \; MPa < P < 18.2 \; MPa$$

$$r_b(^{mm}/_s) = 5.14675[P(MPa)] - 101.007 \; for \; 18.2 \; MPa < P < 40.8 \; MPa$$

$$r_b(^{mm}/_s) = 11.04[P(MPa)]^{0.679} \; for \; 40.8 \; MPa < P < 102 \; MPa$$

Chemistry in the low-pressure regime has been extensively studied and is well understood. The chemistry of the higher-pressure burning regimes is less studied. Turbulence is the dominating driver of flame speed at these pressures, so chemistry studies have been suspended in place of more experimental in-situ research.[24]

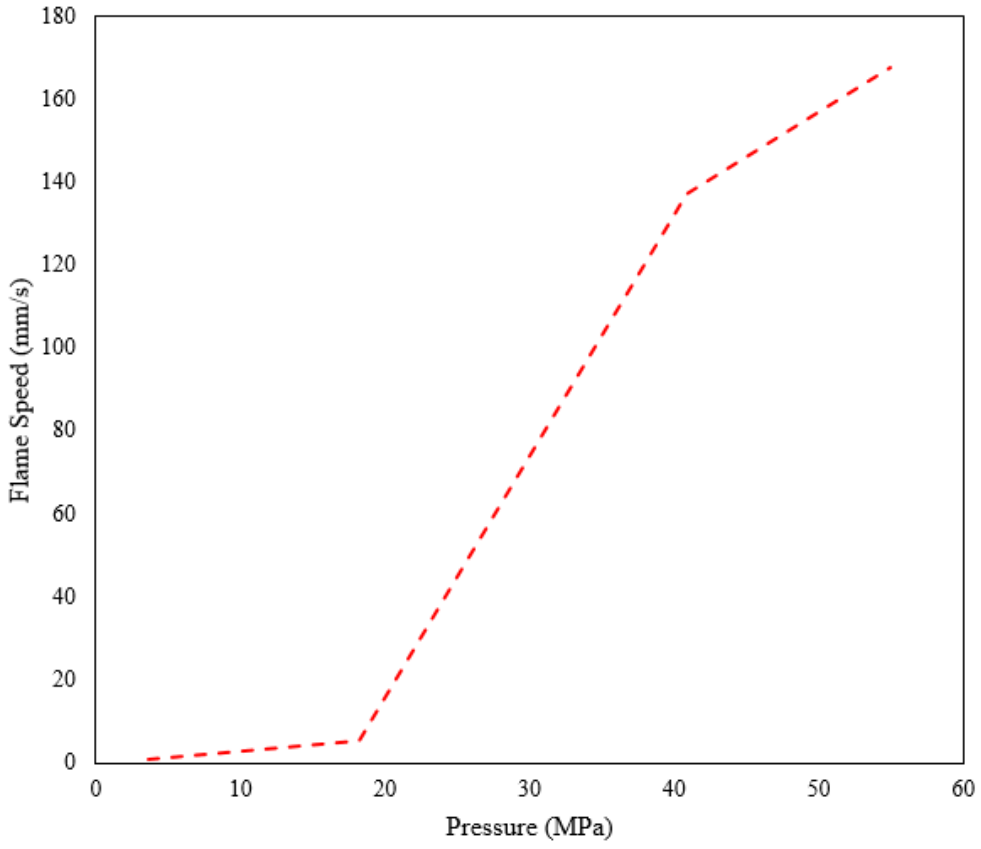

Figure Three: Flame Speed of Nitromethane as a Function of Pressure

1.4 Research Methods

In order to meet the objectives outlined above, a plan was developed to perform this research. Chapter two outlines the background information behind nitromethane and its decomposition. This includes a literature survey, describing former research on nitromethane flames and the chemistry behind it, as well as other reaction mechanisms. These important sources give the basis for mechanism development, both in examining former mechanisms and proposed reactions of nitromethane, as well as comparable reactions and decomposition mechanisms of similar chemistries.

Chapter three defines the methods of computational chemistry used to begin the bottom-up approach to determine the reaction set to be appended to the baseline mechanism. This includes ab-initio methods, density functional theory (DFT), and reactive molecular dynamics. Most of the data extracted from the simulations performed was from ReaxFF, so chapter four was dedicated to the reactive molecular dynamics data set. Speciation data were taken from ReaxFF and is defined as a comprehensive set of reactions and discussed in detail.

The reaction set derived from the ReaxFF data is distilled down and described in chapter five, along with the assumptions and approximations that were used. Added species are discussed, along with implications of these additional reactions. Other aspects of chemistry that were examined and included, beyond the initiating reactions described in chapter five, are discussed in chapter six. This includes a background on soot formation and an associated mechanism used to assess this in the nitromethane flame, as well as a background on carbon

chemistry and included C_2 reactions from the GRI Mech 3.0. Chemkin data, particularly temporal domain and ignition delay solution data, are discussed in chapter seven.

CHAPTER TWO

Background and Review

Nitromethane has been studied for well over a century, with important fundamental research being done by Aerojet, funded by the Office of Naval Research (ONR) in 1954.[25] In this study, evidence was presented for the presence of formaldoxime in the thermal decomposition of nitromethane. This intermediate has proven to be of interest in the reaction mechanism being developed in the current research. The Aerojet study was done on low pressure liquid nitromethane in the context of rocket engine fuel, and the determination of a mechanism was performed for the purpose of studying ignition delay times. In 1995, Melius published a comprehensive study of the thermal decomposition mechanism of nitromethane, examining the thermochemistry of the reaction and species involved as well.[2] This has become an extensively used and accepted anaerobic decomposition mechanism for nitromethane. It includes enough elementary reaction steps such that it is versatile and encompasses many of the important aspects of this monopropellant flame, yet it has few enough species and steps that it is not computationally expensive to run.

2.1 Nitromethane Reaction Literature Review

One of the earliest studies examining the thermal decomposition chemistry of nitromethane propellant was performed by Taylor and Vesselovsky in 1934.[26] In their study, they examine the pressure increase of isothermal decomposition across a range of temperatures between 380°C and 420°C and

initial pressures of 24.5 to 201 mmHg (0.47 to 3.89 psi). The effect of additional gases on the reaction were studied, particularly helium, nitrogen, nitric oxide, carbon dioxide, and oxygen. Only oxygen was reported to have an appreciable effect on the thermal decomposition. Taylor and Vesselovsky report an apparent activation energy of sixty-one kilocalories per mole, and speculate that the initiation step occurs as

$$CH_3NO_2 \rightarrow CH_3NO + \frac{1}{2}O_2$$

They justify this reaction by the formation of nitrosomethane, which was demonstrated by the reflux of boiling nitromethane for two days. After this, they found a portion of the reflux boiled at 84°C (183°F), which is the boiling point of formaldoxime, which is structurally isomeric with nitrosomethane and is known to be more energetically stable. Further chemical testing was done to prove the presence of formaldoxime. Nitrosomethane was also postulated to combine with a methyl radical and decompose into ethane and nitric oxide.

In 1950, Cottrell, Graham, and Reid continued this study.[27] They propose an initial mechanism involving carbon-nitrogen bond fission, with an activation energy of fifty-three kilocalories per mole, as follows

$$CH_3NO_2 \rightarrow CH_3 + NO_2$$

This is in disagreement with Taylor and Vesselovksy, claiming that this reaction is more energetically favorable. In this study, a double-beam infrared spectrometer was used to examine the gaseous products. Species noted include CO_2, C_2H_6, C_2H_4, N_2O, CH_4, NO, and CO. Sodium nitrate was also observed, and

its presence was justified by chemical attack of the product species on the rock salt cell windows. Also of note is that in the final species, C_2 species were present at approximately an order of magnitude less than CH_4. These experiments tested reaction rate at higher pressures than Taylor and Vesselovsky, at pressures between forty and 400 mmHg (0.77 to 7.74 psi), though rates between the two published works are in good agreement. Hydrogen abstraction is speculated here, with a methyl radical being the deprotonating agent for nitromethane. This comes from an analogous reaction, cited within the paper, for the deprotonation of an oxy-hydrocarbon species by a methyl radical for the formation of methane gas. The last notable part of this research is the disproportionation reaction of methyl radicals to the formation of methane and carbene. The presence of carbene, either singlet or triplet, can lead to higher carbon chemistry through fragment recombination, a gateway mechanism to soot formation.

Aerojet-General Corporation in 1954, on behalf of the United States armed forces, investigated Nitromethane decomposition in the explicit context of rocket combustion.[25] At pressure of 250 psia, Aerojet examined the thermal decomposition of nitromethane using mass-spectroscopy. Formaldoxime was found present in the initial decomposition of the fuel, supporting the original work of Taylor and Vesselovsky in their proposed nitrosomethane formation, with rapid rearrangement to the more stable formaldoxime isomer. The nitrogen part of the decomposition chemistry was determined to vary greatly from test to test, demonstrating complex and extensive chemistry. This report also disregards the assumptions made by Graham, Cottrell, and Reid that led them to select their

initiation mechanism over the one proposed by Taylor and Vesselovsky, particularly those regarding formaldoxime, nitrosomethane, and their structural analogues acetamide and acetaldoxime being energetically analogous as well. Direct formation of formaldoxime was proposed through rearrangement of the nitro group via hydrogen bonding between an oxygen atom and a proton, similar to the methyl nitrite rearrangement mechanism discussed in a later paragraph of this section.

Mueller studied nitromethane decomposition at nearly the same time as Aerojet, in a similar range of initial conditions (355°F and 180-300 psia).[28] Isothermal decomposition was studied, and reported species include CO_2, CO, CH_4, HCN, CH_3CN, C_2H_5CN, CH_2O, NO, N_2O, N_2, and H_2O. The results of this paper support the previous work of Aerojet, where oxygen dissociation and carbon-nitrogen bond fission have the potential to happen in tandem as an initiation mechanism. However, Mueller makes the distinction that there are particular initiation regimes as a function of pressure, where carbon-nitrogen bond fission is the predominant mechanism at low pressure, and oxygen abstraction and formaldoxime rearrangement is the driving mechanism at high pressure. He also emphasizes the importance of hydrogen cyanide in this reaction, mainly due to its prolonged presence as a product species in large quantities.

Makovky and Gruenwald of Hafia, Israel in 1958 continued this work, observing a yet lower activation energy of 49.2 kilocalories per mole for the overall reaction.[29] A solid was also found in these experiments, empirically of

$C_{10}H_{10}N_4O_2$ composition. They disagree with Mueller and claim that oxygen dissociation and formaldoxime formation is not a viable initiation step because it is not energetically favorable, but do not appear to give much support or evidence to this statement. The experimental portion of the study examines decomposition at pressures up to forty-one times atmospheric pressure (603 psia), and focuses mainly on hydrogen cyanide formation and its chemistry in the nitromethane flame. Cyanide chemistry is prevalent in the nitromethane flame that is devoid of additional oxidizer to aid in complete combustion, and Mueller attests the large quantity of cyanide present is from formaldoxime decomposition. Makovky and Gruenwald claim that nitrosomethane and, in turn, formaldoxime are formed from methyl radical and nitric oxide recombination rather than oxygen dissociation from nitromethane and rearrangement, providing an alternate explanation to the formation of cyanide than the one presented my Mueller.

C. Melius, working out of Sandia National Laboratories, published on a now widely accepted nitromethane thermal decomposition mechanism.[2] Melius developed a finite rate mechanism in order to study ignition delay times for nitromethane, and distills his full mechanism down into an abbreviated global mechanism. The full mechanism included forty-eight species, and initiates via fission of the bond between the carbon and nitrogen atoms. Once dissociated, a common nitrogen monoxide elimination pathway is through rearrangement to methyl nitrite, where the nitro group reattaches to the methyl group by one of the oxygen atoms rather than the nitrogen atom. Methoxy radicals, left behind after the nitrogen monoxide elimination, oxidize further to formaldehyde and generate

hydrogen gas in the process. The oxidation continues similar to typical hydrocarbon combustion processes, generating carbon monoxide and finally carbon dioxide. It is important to note that, unlike common hydrocarbon combustion mechanisms such as the GRIMech, chain fragment recombination is not present in Melius' mechanism. None of the forty-eight species in the mechanism include any molecules of chain C_2 or greater. This is presumably due to the rather direct conversion of most CH_3 radicals to CH_3O, with the rest being converted to methane or methanol, and oxidizing in similar pathways to CH_3O toward final product species. It can also be attested to the low concentration of hydrocarbon radical species relative to a typical hydrocarbon combustion mechanism for species such as propane or iso-octane.

Glarborg, Bendtsen, and Miller in 1998 studied the chemistry of nitromethane dissociation, particularly in examination of the carbon-nitrogen bond fission reaction.[30] In the dataset published, nineteen reactions involving the initiation and early reaction stages of nitromethane were examined. Glarborg et al. observed that nitromethane commonly interacts with atomic hydrogen, atomic oxygen, and hydroxyl radicals in its own deterioration. Some paths examined lead to the formation of nitrosomethane, and many others lead to the formation of a deprotonated nitromethyl radical. This comprehensive study of nitromethane initiation and consumption reactions utilizes bond-additivity-corrected calculations with fourth order Moller-Plesset perturbation theory (BAC-MP4) level calculation.

Boyer in 2005 extensively studied the burn rate characteristics of nitromethane fuel in an anaerobic environment across a range of pressures from three to 170 megapascal (435 to 24,656 psi).[1] In this study, Boyer developed and used a chemical mechanism derived from the work of Glarborg, Bendtsen, and Miller, as well as the cyclotrimethylenetrinitramine (RDX) decomposition mechanism of Yetter, described in section 2.2.[30][31] Using this mechanism, combined with a gasification model to simulate the regression of the liquid-gaseous interface for sub-critical liquid nitromethane combustion, Boyer was able to describe sub-critical burn rates with reasonable accuracy. Derk continued this work, looking at experimental burn rates more accurately between 3.6 and 101.7 megapascal (522 to 14,750 psi).[24] The chemical mechanism alone does a poor job describing the burn rate near and above 18.2 megapascal (2640 psi). In this region, the flame burns with great turbulence, and it has not yet been determined experimentally if there is a change in chemistry in the turbulent flame speed region of nitromethane.

Han, van Duin, Goddard, and Strachan in 2010 studied the thermal decomposition of nitromethane using ReaxFF reactive molecular dynamics simulations.[32] This study explicitly examined the liquid and solid phases, with temperatures from 2000 to 3000 Kelvin and a density of 1.97 grams per cubic centimeter. The initiation event examined in this study was the intramolecular rearrangement to methyl nitrite, though intermolecular proton transfer was also observed. The disproportionation of nitromethane to CH_2NO_2 and CH_3NOOH has a calculated charge transfer of approximately 20% standard electron charge,

which was reported to be in good agreement with previously calculated results of quantum-mechanical simulation. This indicates that the proton transfer reaction is likely non-ionic, and does not follow a heterolytic reaction path.

Rom, Zybin, van Duin, Goddard, Zeiri, Katz, and Kosloff continued this work using the same reactive molecular dynamics methods in 2011.[33] This study particularly focuses on liquid nitromethane and its initiation through adiabatic compression. It was observed that the low pressure/low compression (<30% compression) case initiates via traditionally examined reactions, including carbon-nitrogen bond fission, methyl nitrite rearrangement, and potentially oxygen dissociation. At compression levels higher than 30%, the initiation was found to occur through either hydrogen abstraction or oxygen abstraction of nitromethane, both forms of nitromethane disproportionation. Previous research on nitromethane performed by Shaw, Decarli, Ross, Lee, and Stromberg supports the hydrogen abstraction initiation at high pressures and densities.[34] A kinetic isotope effect was observed in deuterated nitromethane, slowing the standard reaction by a factor of ten. This implies that the proton on nitromethane that was replaced with deuterium is strongly involved in the affected reaction.

2.2 Combustion Mechanism Development Literature Review

Anderson et al. at the US Army research laboratory developed a very comprehensive study of dark zone finite rate kinetics.[35] The mechanism published was developed for the investigation of the dark zone in gun propellants, mainly double base propellants consisting of nitrocellulose and nitroglycerin, as well as the dark zone in nitramine and nitrate ester flames. The

dark zone is the non-luminous region of these flames that is observed at low pressures (less than one-hundred times atmospheric pressure). This region has low molecular weight and highly diffuse species that occur in the intermediate chemistry, such as NO_x compounds, cyanide derivatives, nitric acid derivatives, amine radicals, and light carbon species of C_1 and C_2 form. The diffuse and reactive species in this part of a propellant flame tend to heavily influence and control the flame speed and flame structure.

Anderson et al. also developed a comprehensive mechanism for monomethyl-hydrazine combustion with red fuming nitric acid as the oxidizer in 2010.[36] These two species form a hypergolic bipropellant with high energy density, an excellent combination for rocketry. The developed mechanism was intended for use with computational fluid dynamics codes in order to simulate complex reacting flow fields. The mechanism includes much of the previous dark zone chemistry work, as well as a large amount of complex chemistry from species too large to be prevalent in the dark zone. The complex carbon and nitrogen chemistry involved in this reaction, including some select nitromethane reactions, provides an excellent dataset to study while developing the initiation mechanism described herein.

Yetter et al. at Princeton University in 1995 developed a model for the simulation of RDX and octogen (HMX) gas phase decomposition.[31] Similarities in decomposition chemistry between RDX, HMX, and nitromethane are expected despite the later being a nitro-hydrocarbon rather than a nitramine species. Yetter predicts multiple viable decomposition pathways for RDX, consisting of

spontaneous de-trimerization or a nitrogen dioxide elimination pathway. If the reaction proceeds through the later initiation step, then nitrous acid elimination, nitrogen dioxide elimination, or decomposition into H_2CNNO_2 and H_2CN pathways present themselves. H_2CNNO_2 then decomposes to form a plethora of small species such as hydrogen cyanide, nitrous acid, nitrogen dioxide, and protonated hydrogen cyanide. H_2CNNO_2 is sensitive to water or hydroxyl radicals, which bond through hydrogen bonding pathways to the nitro group side of the molecule, causing destabilization and catalyzing rapid decomposition to formaldehyde and nitrous oxide. Once decomposed into these small, diffuse molecules, a dark zone forms and chemistry as described by Anderson et al. proceeds to occur.

Pitz and Westbrook in 2007 developed a mechanism for the decomposition of well-known explosive tri-nitro toluene (TNT) working at Lawrence Livermore National Laboratory (LLNL).[37] This mechanism breaks down via nitrogen dioxide elimination, leading to dinitrobenzene and NO_2. Disproportionation can occur here, leading to an oxidized dinitrobenzene radical and nitric oxide. Decomposition following this pathway leads to soot formation, as nitrogen dioxide and nitric oxide molecules remove themselves from the fuel, leading to benzene with active radical sites where the nitro groups have removed themselves. This leaves a direct pathway to polycyclic aromatic hydrocarbon formation and sooting, as opposed to RDX, which is observed to burn cleanly due to its minimal C_1 carbon chemistry.

2.3 Nitromethane Chemistry

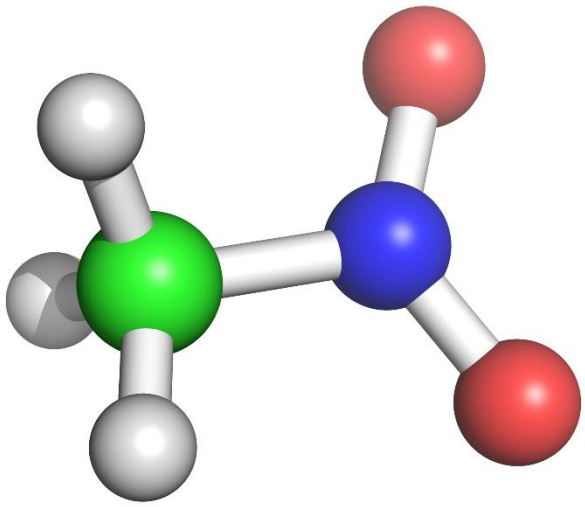

Figure Four: Ball and Stick Model of Nitromethane

Nitromethane is a simple organic molecule, consisting of only seven atoms, four elements, and two basic functional groups joined across a single bond. Ab-initio and DFT analysis shows that the sp^3 hybridized carbon in the methyl group has three single bonds to the hydrogen atoms, and one single bond of reduced strength to the nitrogen bond.[38][39] The two oxygen atoms attached to the nitrogen atom have diminished second order bonding character (or enhanced first order bonding character), indicative of a resonant stabilization. The oxygen atoms exhibit a weak bonding character to each other, less than one-quarter bond order, also indicative of resonant stabilization across the nitro group. This is likely an artifact of the simulation and the way Mayer bond orders are calculated,

since the calculation shows the bond angle between the oxygen atoms is wide and the distance is far. Nonetheless, this calculated partial Mayer bond order does indicate added stability in formation enthalpy of the nitro group. Table one shows the Mayer bond order analysis of the nitromethane molecule, taken from a computational DFT analysis done in ORCA using the B3LYP exchange-correlation functional and the 6-311+G* basis set.

Bond Number	**Bonding Atoms**	**Mayer Bond Order**
1	C-N	0.6949
2	C-H	0.9142
3	C-H	0.9266
4	C-H	0.9054
5	N-O	1.7580
6	N-O	1.7630
7	O-O	0.1198

Table One: Mayer Bond Orders of Nitromethane from DFT/B3LYP Results in ORCA

Löwdin charge and Mayer population analysis further supports evidence of resonance as the main thermodynamic stabilization mechanism in the nitro group. Polarity within the molecule and weak potential acidity of the hydrogen atoms on the methyl group are also evident in the analysis, both of which play an important role in the current proposed initiation mechanism that is hypothesized to occur at high densities, the effects of which will be discussed in chapter five.

Atom	Löwdin Partial Charge	Mayer Total Valence	Mayer Bonded Valence
C	-0.2883	3.4638	3.4638
N	0.0936	4.1397	4.1397
O	-0.1870	1.8849	1.8849
O	-0.1841	1.9317	1.9317
H	0.1888	0.8781	0.8781
H	0.1849	0.8822	0.8822
H	0.1921	0.8779	0.8779

Table Two: Population Analysis of Nitromethane for DFT/ B3LYP Results in ORCA

CHAPTER THREE

Computational Chemistry Methods

Described in this chapter are the computational chemistry methods used in the bottom-up approach taken in the development of this high-density initiation mechanism for nitromethane. Like many other aspects of engineering simulation and the tools that are available, there are strengths and weaknesses to each method. Ab-initio and DFT methods are described first, and are the methods used to define the species and reactions observed in the ReaxFF molecular dynamics simulation. These methods, though computationally expensive and time consuming to perform, are highly accurate and offer valuable insight into the thermodynamics of the observed reactions. Later described is the ReaxFF method that was implemented and used to run molecular dynamics simulations. This method captures the critical aspects of ab-initio and DFT simulation and distills them down into a less computationally expensive simulation that can be run for longer duration. Value here comes in the form of time; longer simulations allow the user to observe larger sections of the transient system. Longer simulations tend to converge on more accurate system descriptions because there is more time for events to occur and, statistically, rare event data is less skewed than it would be in a shorter simulation.

3.1 Ab-Initio and Density Functional Theory Methods

Ab-initio methods for computational chemistry were developed from fundamental principles of physical chemistry and quantum mechanics. These

numerical and computational methods were developed in order to solve the Schrodinger equation for systems containing more than one electron. Analytical exact solutions for the electronic Schrodinger equation only exist for systems with one electron due to the incapability to exactly define the electron-electron repulsive potential in the expanded Hamiltonian operator. The Hartree-Fock approximation states that electrons can be assumed to move independently of each other.[40] Mathematically this manifests itself as an expansion of the electron-electron repulsion term as a series of atomic orbitals, to each of which a single electron is assigned, and each electron sees a mean repulsive field as a representative force from all the other electrons in the system. This approximation is the basis of the original ab-initio method, known as the Hartree-Fock (HF) method. In the Self-Consistent Field (SCF) algorithm, the molecular orbitals (as defined by the spin orbitals that the electrons are assigned to) are continuously varied until the energy state of the system is minimized. This energy minimum is the calculated zero-point energy of the system, or the numerical ground state solution for the system of atoms being examined.

Traditional Pauling-Slater valence bond theory, though sufficient for simple molecules, has difficulty describing polyatomic molecules and doesn't adequately define more complex systems or geometries.[41] Molecular orbital theory was developed in order to more completely describe complex systems of bonding atoms.[41] In this theory, molecular orbitals are generated and defined as a linear combination of atomic orbitals. This superposition theory stems from the assumption that near the nucleus of an atom, an electron will most closely

resemble its atomic orbital wavefunctions, and unlike valence bond theory, are not bound tightly to bond spaces between atoms. From this superposition, the concept of bonding, antibonding, and non-bonding orbitals arose. Single electronic wavefunctions can add in three different ways. A bond is formed when the wavefunctions add constructively, creating a space of enhanced electron probability between nuclei and allowing delocalization and transfer of electron density. Conversely, an antibonding orbital is generated when wavefunctions add destructively, creating a nodal place between nuclei that electrons are not able to cross and ultimately end up shifting charge density away from the antibonding node. Lastly, wavefunctions can add completely out of plane and phase, having no additive effect on each other; this is the case with a non-bonding orbital space.[41] Wavefunction behavior, and the use of superposition allows for computational methods to be used that vary geometry and calculate the weighting coefficients for these linear combinations, leading to a self-consistent energy minimization algorithm.

Traditional HF methods are limited in that their total energies, or the formation enthalpy from the computation, will be too positive since the calculated electron-electron repulsion energy will be too large.[42] The difference between the exact energy of the system and the energy calculated by the HF methods is called a correlation energy. Correlation energy is a correction factor applied to the original Hartree-Fock approximation that all electrons move independently of each other. Electrons do not interact solely with an electric field; this is a simplified representation of the other electrons in the system. The

electrons will instead interact with each other and correlate their own paths relative to the others. This correlation energy, therefore, is a reduction in the total energy that allows an HF analysis to converge upon the exact solution of the Schrodinger equation.

The basis sets, or atomic orbital representative wavefunctions, that are chosen have a large influence on these calculations. Atomic orbitals are inherently described as slater-type orbitals (STO), which are functions that decay exponentially as the electron moves away from the nucleus.[43] STOs also have a cusp at the origin where the electron approaches and overlaps with the positively charged nucleus. Despite the realistic accuracy of this type of orbital, they are seldom used. The cusp at the origin presents a discontinuity in the function, posing difficulty in performing the necessary calculus for numerical solutions, and the exponential decay similarly increases computational cost of these functions. Gaussian-type orbitals (GTO) were created to replace these STOs. A summation of multiple GTOs is used as an approximation of an STO, with the added improvement that gaussian curves are much more easily differentiable and decreases computational cost significantly.[43] These are known as minimal basis sets. The addition of higher order unoccupied orbitals (p, d, and f orbitals in the series) are called polarization functions and, although they increase computational cost, tend to increase accuracy for systems with dipoles and electronegativity gradients. More complex basis sets are generally used for acceptable accuracy in HF and post-HF calculation methods, such as split valence basis sets. Based on the assumption that the valence electrons are the ones that

participate in bonding, the valence shell and core shell electrons are broken apart and treated differently, allowing for more computational power to be expended selectively on defining the valence shell electrons, while acknowledging that the closed inner shell electrons maintain resistance to polarize away from their atomic orbital form.

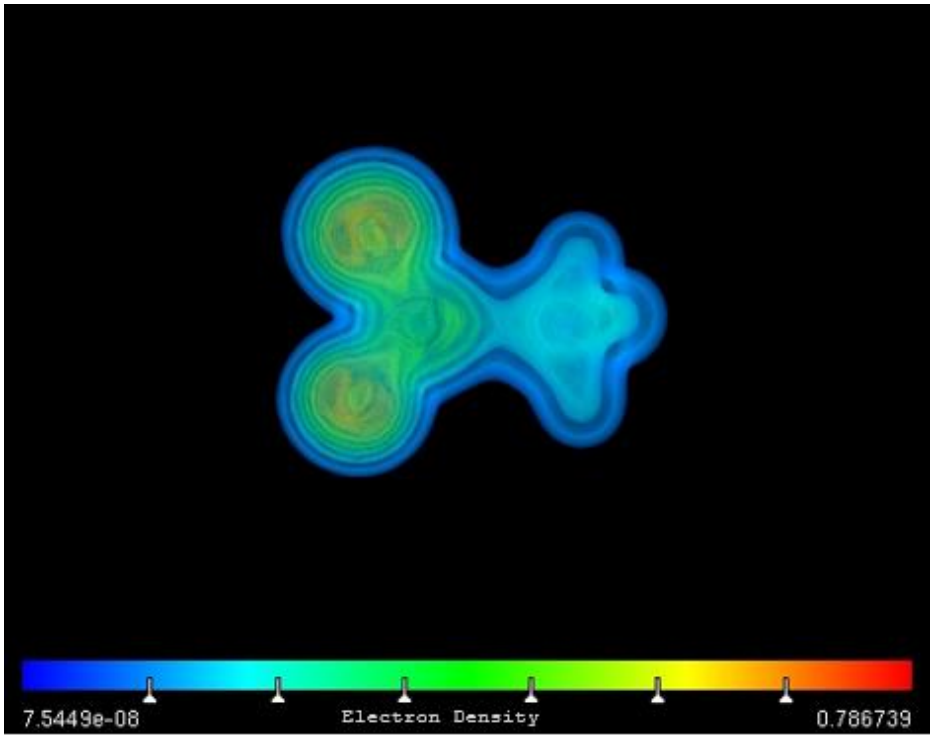

Figure Five: Electron Density Map of Nitromethane from Ab-Init

Density Functional Theory (DFT) calculations came to be after Hartree-Fock methods were developed, revolutionizing computational chemistry. DFT is based on the premise that the system can be defined solely by a functional of charge density, describing the complete electronic structure of the molecule.[44] An example of DFT-level simulation output is shown in figure five. Pictured is a geometry optimization of the nitromethane molecule at the 6-311+G* level with

GGA exchange-correlation method, showing the electronic shell structure of the molecule.[42][44] The color-scale depicts the relative electron density across the space of nitromethane.

3.2 Reactive Molecular Dynamics

Molecular Dynamics (MD) simulations are a method of running complex simulations of systems of atoms and molecules by solving all positions and energies based on a force engine. The force engine can be ab-initio based, solving these QM methods directly and stepping through time in order to solve trajectory and energy for all particles in the system. Another method that yields faster results is to use an empirical force field based on ab-initio data collected from more fundamental computational methods. This is accomplished by simplifying molecules into basic mechanical equivalents and fitting pseudo-mechanical parameters to both quantum mechanical (QM) data and experimental thermodynamic data.[42][45] Empirical force fields have the potential to extend the simulated time of these non-continuum systems over ab-initio force engines while reducing the full computational cost.

In traditional force-field based MD simulations, reactivity is not considered, and the molecules defined initially are maintained throughout the course of the simulation. This allows for uncomplicated definitions of molecules, where all bonds can be treated as simple harmonic oscillators and spring constants can be curve fitted from calculated compressibility data.[42][45] Other forces in the system are based on simple electronic attraction and repulsion terms, where each atom has a charge associated with it based on the partial

charge calculated in ab-initio simulation. These repulsion and attraction terms will yield dynamic behavior between separate molecules, as well as forces associated with steric strains within a molecule between its own function groups, all summing in addition to kinetic elastic collisions. This type of simulation is useful in examining effects such as phase separation and phase change, mass diffusivity, thermal diffusivity, and viscosity. For capturing reactivity, however, a more complex simulation method is required for development of finite rate kinetics.

ReaxFF, a reactive force field method developed by van Duin. et. al. was used in the MD simulations run herein for the purpose of collecting and developing finite rate kinetics data, and examining anaerobic decomposition pathways of nitromethane propellant. ReaxFF differs from traditional MD in that bonding is considered at every timestep in the simulation, and calculated from a bond order correlation based on interatomic distances for every atom in the system. This means that all atoms are treated individually, regardless of hybridization, coordination, or bonding scheme.[46] Force fields are developed for specific sets of systems, similar to traditional MD force fields, and are trained to known or calculated datasets. ReaxFF is ideal for examining reactivity in supercritical combustion, particularly since high-temperature and high-pressure simulations run far faster than ones run at low pressure and temperature. The force field chosen for this study was developed and optimized for the combustion of high energy explosives, such as RDX and Pentaerythritol tetranitrate (PETN), and was verified using nitromethane combustion as a standard.[47]

3.3. Simulations and Extracted Data

3.3.1 ReaxFF

Simulations were run using the ReaxFF reactive molecular dynamics interactions and methods, as implemented in the LAMMPS engine developed by Sandia National Laboratories.[48][49] These simulations were run at a variety of supercritical densities in order to determine an estimate for the transition point between the traditionally accepted initiation mechanism of nitromethane and the one proposed within this paper. A supercritical fluid is one which, above its supercritical temperature and pressure, forms a phase that is neither liquid nor gaseous. In this state, the compound exhibits real gas properties and is highly non-ideal, but in the absence of a two-phase interface, the flame is free to propagate rapidly uninhibited by the evaporation rate of the liquid.

The initial supercritical density required for hydrogen abstraction initiation was found to be approximately 0.83 grams per cubic centimeter. This value was found by running an initial energy minimization on nitromethane systems of various densities, and then running the molecular dynamics simulation for short times (<50 femtoseconds) in order to observe the cross-over point between reaction and no reaction. Systems with this initial density were then run at 600K and 800K initial temperatures for tens of picoseconds. Within this time, species were examined and reactions were recorded as potential addendum to the mechanism used by Boyer, amending the initiation scheme at high densities to properly reflect laminar flame speed and ignition delay times. Due to the more intensive level of simulation performed using this computational

chemistry tool, the ReaxFF simulation set will be discussed further in depth in chapter four.

3.3.2 ORCA

Simulations were performed using ORCA, an ab-initio and DFT computational software package, for five species involved in the appended initiation: nitromethane, a nitromethyl radical, protonated nitromethane, methyl nitrate, and a protonated nitromethyl radical.[38][43] A triple zeta (three basis functions for each atomic valence orbital), split valence Pople basis set with included polarization and diffuse functions (6-311+G*) was used in the initial ORCA DFT calculations, solving a geometry optimization problem prior to normal mode analysis.[38][43] The Pople basis set, though potentially less accurate than the equivalent triple zeta Dunning basis set for more intensive calculations such as correlation consistent analysis, is ideal for DFT calculation because it provides sufficiently accurate analysis at a greatly reduced computational cost.[43]

Three other species were examined in the same manner; CH_3O_2, CH_3OOH, and CH_2O_2. These species were observed in the reactive molecular dynamics simulation and their presence has been noted in other published mechanisms, such as Pitz and Westbrook's Trinitrotoluene decomposition mechanism.[37] DFT analysis of these three species was performed in order to assess the relative formation energy of these species, both to each other and to the other species analyzed. This served as verification that the presence of these species was plausible and not simply and artifact of the ReaxFF simulation and the method used to sample speciation data.

Materials studio and the DMol3 QM package were used to investigate the formation energy of constitutional isomers of CH_3NO; in particular, the regioisomers H_3C-N=O and H_2C=N-OH. In order to use ORCA accurately to study these species, a large basis set (6-311+G*) was used and a post HF method using Mollier-Plesset second order (MP2) perturbation was tried. This posed an issue; computational time was prohibitively long (did not converge over multiple days on a personal computer), so DFT methods were used instead, and are believed to be of reasonable accuracy. More detailed information on ORCA simulations and calculations, such as homolytic bond dissociation energies, will be discussed in chapter five alongside the initial reaction dataset.

CHAPTER FOUR

ReaxFF Simulation Data

ReaxFF simulations were run extensively using the Sandia Large-scale Atomic/Molecular Massively Parallel Simulator (LAMMPS) molecular dynamics engine on a personal laptop for the purposes of collecting data in supercritical nitromethane flame data, as well as validating the force field and looking for accuracy indicators.[46][48][49] This was done by looking through the speciation data outputs of the simulation and checking for apparently incorrect or impossible species. A sample of the output data is presented in Appendix B, and simulation input data for ReaxFF/LAMMPS is given in Appendix C. Nothing of note was observed in terms of erroneous data or inaccuracy indicators, and the extracted data will be discussed in this section.

4.1 Initial Simulation Set

The initial simulation set investigated utilizes the high energy force field developed by Strachan et al for simulating shock waves in nitramines such as RDX.[47] The updated force field of van Duin et al. was not selected because of its inclusion of silicon atom chemistry. This force field was developed for investigating the sensitivity of pentaerythritol tetranitrate (PETN) relative to its silicon-based derivative.[50] Though more accurate for species of this nature, the original force field for C, H, O, and N based species optimized for RDX is much more appropriate for examining nitromethane decomposition. The low-gradient

(LG) force field of Liu et al. was used in some early simulations, but was quickly discarded due to its over-prediction of reactivity at the simulated conditions.[51]

The first simulations were performed as canonical and microcanonical simulations (NVT and NVE, respectively), used to examine a freely expanding flame at various temperature contours throughout the flame.[46] Though informative, these simulations did not provide the level of insight needed to develop a reaction set addendum to the baseline mechanism. They did, however, show that under the proper conditions, hydrogen atom abstraction was the primary initiation mechanism. This reaction occurs much sooner in the flame, indicating a reduced ignition delay time relative to the currently accepted carbon-nitrogen bond scission initiation.[1][2] However, at later points in the flame, these two mechanisms were observed to occur in tandem. The remaining simulations were run as NPH (fixed pressure-enthaply) simulations, and started as NPT (fixed pressure-temperature) to equalize the initial state of the system. The NPT timesteps were set orders of magnitude lower than the main simulation timesteps such as not to be intrusive to the NPH simulation. A conjugate gradient energy minimization starts the simulation, followed by five femtoseconds of NPT equalization, and then ten picoseconds of NPH simulation. These simulations were run for a variety of initial densities between 0.65 grams per cubic centimeter and 0.87 grams per cubic centimeter, and it was found that 0.83 grams per cubic centimeter was the critical density that above which, hydrogen abstraction initiation occurs. These simulations do exhibit some sensitivity to the initial condition of the system, inherent to the method used in LAMMPS to set up the

starting configuration. Special precautions were taken when setting up the initial system of atoms and initial conditions were iterated upon such that the density was accurate before the energy minimization step, and that the NPT equalization was only a temperature equalization step and not a density equalization as well. Too high a density before the energy minimization potentially yields a false positive on hydrogen abstraction initiation, and too low a density pre-energy minimization can, similarly, give a false negative on initiation.

The 0.83 gram per cubic centimeter initial density case has results of the most interest for the purpose of developing an addendum initiation reaction set. Within the first eleven femtoseconds of simulation time, the nitromethane fuel begins decomposing via hydrogen abstraction, and within twenty-nine femtoseconds, these hydrogen atoms in the mixture begin to recombine with the nitro-group on existing nitromethane molecules. The hydrogen atoms also rapidly recombine with each other to form H_2 molecules. It is notable that nitromethane does appear to dimerize occasionally throughout the reaction, but this phenomenon was not included in the added reaction set due to its short intermediate lifetime with no forward reaction, and the low energy storage capacity of the hydrogen bonding in the dimer. At ninety-six femtoseconds,

hydroxyl radicals begin to dissociate from CH_2NOOH, leaving H_2CNO behind. This is the earliest point in the flame that a reaction in the hydrogen abstraction

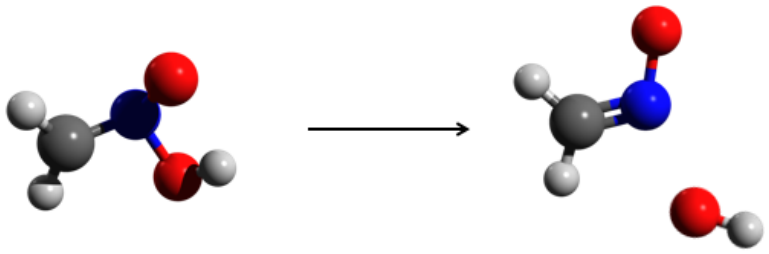

Figure Six: CH_2NOOH Dissociation from ReaxFF

initiation ties into the existing baseline reaction set. H_2CNO is an existing and critical species in the reaction sets of both Boyer and Melius.

From this point in the reaction onward, hydrogen bonding is of noted importance and leads to a large portion of the transition states in the later reactions. Molecular hydrogen and water bind to the nitro-group on nitromethane and its derivatives, and hydrogen binds to water and hydrogen peroxide to form shortly lived pseudo-H_3O and H_3O_2 species. At 199 femtoseconds, protonated nitromethane decomposes in an analogous pathway to nitromethane; nitrous acid (HONO) rearranges and recombines to form a protonated analog of methyl nitrite, and then dissociates into a methoxy radical and HON, which will rearrange to form the more stable nitroxyl isomer (HNO).

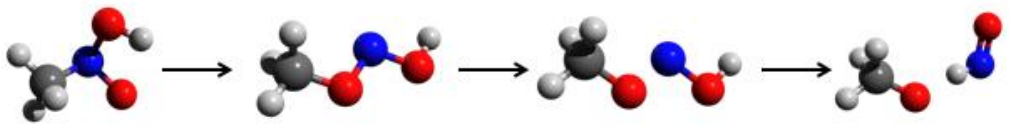

Figure Seven: CH_3NOOH ReaxFF Rearrangement Reaction Diagram

Similarly, CH_3NO is formed through oxygen dissociation of nitromethane, and the hydroxyl dissociation of CH_3NOOH. Within twelve femtoseconds of these events, CH_3NO decomposes into CH_3 and NO, and simultaneously H_2CNO reacts with a proton to form a hydroxyl radical and CH_2N. By 231 femtoseconds of simulation time, carbon-nitrogen bond scission of the remaining nitromethane begins to occur, and the reaction progresses as described by the baseline nitromethane decomposition mechanism of Melius, similar to that of Boyer. The remaining nitromethane analogues decompose through a CH_3NO pathway, with O or OH elimination occurring, and continuing to oxidize through H_2CNO.

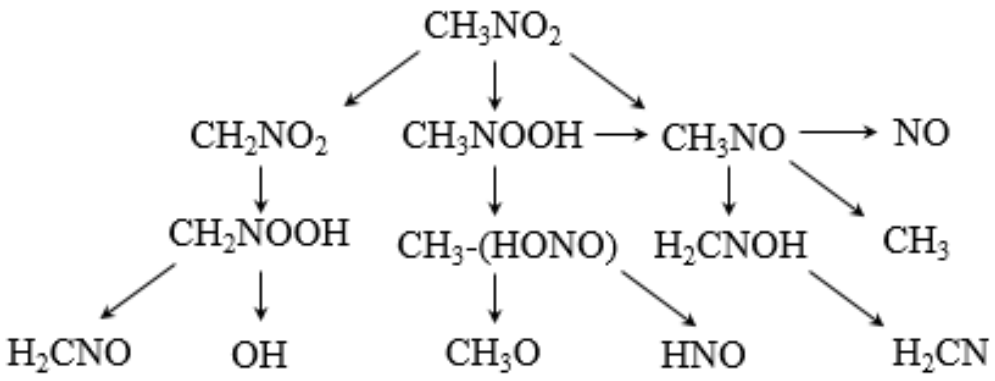

Figure Eight: ReaxFF Nitromethane Decomposition Pathway Visual Map

4.2 Water Sensitivity

Nitromethane is known to sensitize when exposed to a variety of different species. Amongst these are nitric acid, methanol, amines, and water.[52][53][54][55] Methanol is used in typical top fuel racing blends, and amines are used in military applications of nitromethane as an explosive, such as the blend of Picatinny Liquid Explosive (PLX). Nitric acid has been used in place of amines for sensitizing nitromethane in the study of its explosive behavior in a laboratory setting, mainly because of amine species' known carcinogenic nature. Water is an excellent sensitizer from a system-level perspective because it's safe, non-toxic, and is neither caustic nor corrosive, so it poses a relatively simple storage and handling requirement. The sensitivity of nitromethane initiation to water was examined using ReaxFF at a variety of pressures and temperatures, and it was observed that water addition starts the onset of hydrogen abstraction initiation at a lower initial density.

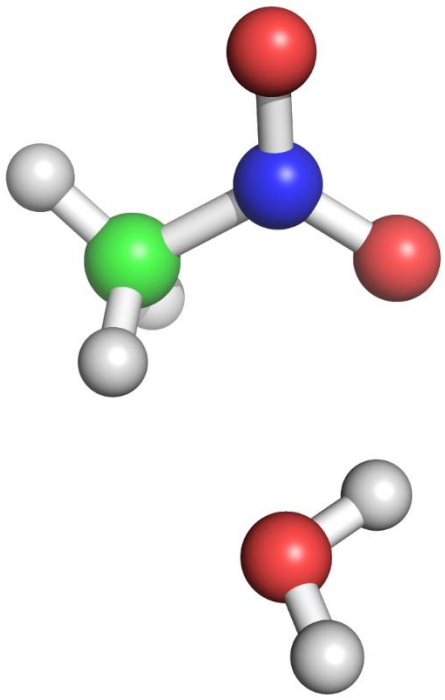

Figure Nine: Ball and Stick Model of Water-Nitromethane Hydrogen Bonding Energy Minimization

In these simulations, water immediately hydrogen bonds to a nitromethane molecule, forming a six-center intermediate complex. The calculated energy of this hydrogen bond is on the order of forty kilocalories per mole, an immense energy for a typical hydrogen bond, which are normally on the order of five to forty kilocalories per mole, indicating high stability.[56][57] From this transition state, the water strips the bonded oxygen from the nitro group and forms nitrosomethane and hydrogen peroxide. The hydrogen peroxide proceeds to bond back to another nitromethane molecule and undergoes a proton transfer

reaction, creating CH_3NOOH and a hydroperoxyl radical. The reaction proceeds slowly, until the nitromethane undergoes classic initiation via rearrangement to methyl nitrite and dissociation to CH_3O and NO. CH_3NOOH later undergoes hydroxyl radical elimination and forms more nitrosomethane. These hydroxyl radicals then abstract a proton from the nitrosomethane and form water and H_2CNO. These reactions proceed simultaneously with the reactions described in the last paragraph at elevated pressures, but at lower pressures (~360 atmosphere pressure), these reactions occur independent of the previously described hydrogen abstraction reactions.

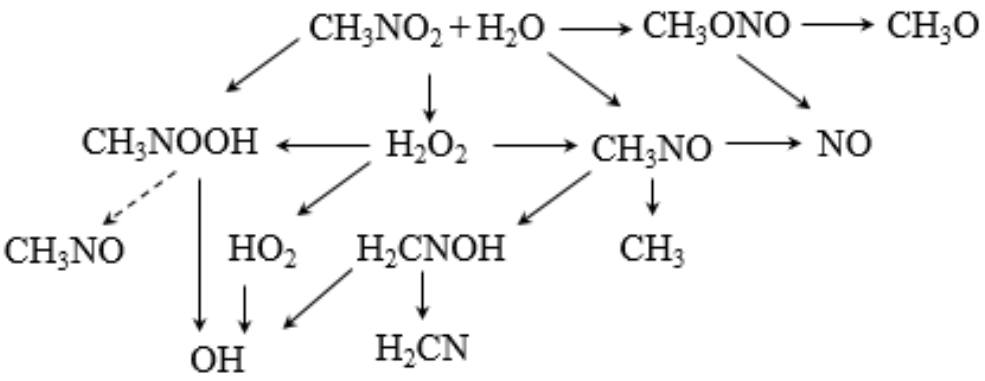

Figure Ten: ReaxFF Water-Sensitized Nitromethane Decomposition Pathway Visual Map

CHAPTER FIVE

Initial Mechanism Development

The data used to develop the mechanism defined here was sourced from multiple references, including Anderson, McQuaid, Nusca and Kotlar's reaction mechanism for mono-methylhydrazine and red fuming nitric acid combustion,[36] Yetter, Dryer, Allen, and Gatto's reaction mechanism for gas phase Nitramine/RDX combustion,[31] and Anderson's reaction mechanism for dark zone kinetics.[35] The existing mechanisms for nitromethane combustion of Glarborg, Bendtsen, and Miller,[30] and Melius,[2] were also referenced for the development of this finite rate mechanism. Thirteen additional elementary reaction steps, given in appendix A, are affixed to the mechanism used by Boyer,[1] along with select C_2 chemistry from GRIMech 3.0.[58]

Unimolecular Reaction Rate Theory

The selected reactions are an abbreviated set of those derived from ReaxFF, set on the basis of unimolecular reaction rate theory. The first practical mechanism for unimolecular dissociation was developed by Lindemann and Christiansen.[59][60] In this mechanism, they examine unimolecular dissociation as essentially a two-step reaction. The reactant molecule undergoes a primary collision with a third body and becomes activated. An activated molecule has enough energy to dissociate stored internally from the collision in the form of vibrational modes.[61] This activated molecule can then either dissociate into product species, or collide with another third body and lose its internal

vibrational energy.[61] Hinshelwood developed this theory further by establishing that the concept of 'activation' is not digital; there are varying degrees of activation.[61] In order to become activated, a molecule must attain an energy that is, at minimum, equal to the activation energy required for the forward reaction to proceed. It is probable that the reaction in which a reactant will become activated to an energy higher than the required activation energy will proceed through collision with a third body, and the probability of this occurring increases with the velocity distribution of the particles in the system. The reaction rate will increase in accordance with the average system temperature since average particle velocity and velocity distribution are functions of system temperature, and the statistically rare event of activation becomes more likely to occur as the average energy of the molecules in the system increases.[61] Hinshelwood therefore made the forward rate constant of the activation step a probability function of temperature. The added level of rigor associated with Hinshelwood's calculation increased the accuracy of the earlier Lindemann-Christiansen theory.[61]

Rice, Ramsperger, and Kassels addressed a shortcoming of Hinshelwood theory; Hinshelwood addressed the variability of the first forward rate constant, but neglected to address the variability of the second forward rate constant. He assumed that regardless of the activation of the reactant molecule, once it was activated to an energy at or above the reaction barrier energy, it would progress forward with the same forward reaction rate constant. RRK theory indicates that this is not true, and that complexes activated to different energy levels above the

reaction barrier energy will progress forward with different forward reaction rates.[61] This is due to the time required for internal vibration modes to shift through a molecule until the energy has concentrated around the dissociating bond. Higher energy molecules contain more internal vibrational quanta, and statistically are more likely to dissociate sooner than molecules with a lesser number of vibrational energy quanta. This theory takes the two-step Lindemann and Hinshelwood theories and makes them a three-step reaction, distinguishing between energized and activated reactant molecules. Marcus developed this theory yet further into the modern RRKM theory by accounting for vibrational quanta using their real vibrational frequencies. This information can be taken directly from ab-initio level calculation, making RRKM theory fully predictive.[61][62]

There are three approaches to handle the treatise of unimolecular dissociation reactions when implementing them into software such as ANSYS Chemkin. The first method is to define the reactions normally, as reversible single step reactions, and attempt to define the reaction parameters via involved ab-initio or DFT level calculation. This may not be the most accurate method across a total range of temperatures and pressures, though Chemkin does include additional optional parameters for pressure centering equations to compensate for this. These pressure centering equations allow for a smooth transition between a low pressure limiting reaction rate and a high pressure limiting reaction rate, transforming the reaction rate-temperature curve from an exponential relationship to a sigmoidal one.[63] The second method would be to

expand each unimolecular dissociation reaction into two or three steps and handle them as multiple, separate, reversible reactions. This comprehensive approach will likely yield the most accurate results across all temperatures and pressures because of its additional rigor and consideration of all possible elementary reaction steps. It is cumbersome though, and adds computational cost to the calculation, along with stiffness to the set of equations to be solved. The third method, used for the calculations done for the purposes of this thesis, was to simplify the dissociation reactions by making them single step, forward only reactions that occur at a reduced rate. This method was chosen for the sake of brevity and simplicity in evaluating the validity of the added reaction set. It forms a pseudo-global reaction out of the multi-step dissociation and maintains low computational cost while capturing the essence of the mechanism.

Homolytic Bond Dissociation Energy

Homolytic bond dissociation energy calculations were performed using ORCA via DFT methods for geometry optimization and energy minimization of product and reactant species.[38] The 6-311+G* basis set was used alongside the B3LYP exchange-correlation function.[43] As discussed in chapter three, other methods were tested but proved too computationally expensive. Two of the reactions examined are the hydrogen dissociation and oxygen dissociation of nitromethane. These reactions have a calculated 105.3 and 94.4 kilocalorie per mole dissociation energy.[64][38] Though higher than the dissociation energy of the carbon-nitrogen bond, these energies are not so much higher that they are not plausible activation pathways. The DFT also does not account for temperature

and pressure effects properly. All simulations were performed on single molecules, with no intermolecular effects included. This makes the simulation most reminiscent of an ideal gas and not fully descriptive of a supercritical real-gas system. Despite this, the single molecule calculation offers valuable insight into the un-influenced species and lays the baseline for realistic predictions to be made. The author postulates that the high density found in a supercritical system causes compression of the initial nitromethane molecule, and this combined with the large dipole moment across the molecule tends to strengthen the carbon-nitrogen bond by localizing electron density and, in turn, reducing the strength of the carbon-hydrogen bond by electromagnetic repulsion of the partially negative nitro-group on the partially positive proton centers. This would make hydrogen abstraction the dominant mode of initiation at elevated density in the supercritical state.

Two other reaction energies were examined with DFT. The first is the hydrogen addition to nitromethane, and the second is the hydroxyl elimination pathway of protonated nitromethane, leading to the formation of

nitrosomethane. The hydrogen addition reaction energy was calculated to be an exothermic 79.84 kilocalories per mole, and the

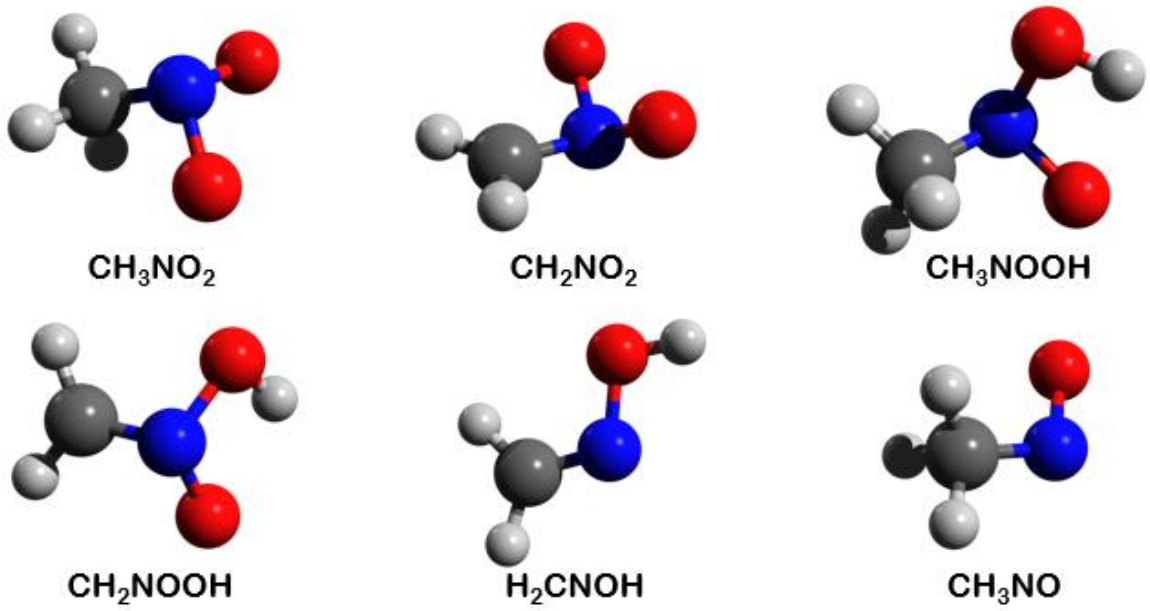

Figure Eleven: Rendered Ball and Stick Model of Nitromethane and its Relevant Analogs

hydroxyl elimination had a calculated dissociation energy of 39.00 kilocalories per mole.[64][38] This energy is far lower than the bond dissociation energy of any of the other three initiation reactions. This means that once the hydrogen dissociation from nitromethane begins to occur, primary initiation is accelerated through the formation of protonated nitromethane, and then hydroxyl elimination to nitrosomethane.

5.1 Reactions

All unimolecular dissociation reactions in this mechanism are assumed to be homolytic, creating a pair of radicals rather than a positive and negative ion.

This form of dissociation creates an energy level between the highest occupied molecular orbital (HOMO) and the lowest unoccupied molecular orbital (LUMO), namely the singly (or semi) occupied molecular orbital (SOMO).[41] This orbital is where the unpaired radical electron resides and is the most important orbital in the potential energy surface around the transition state of the reaction coordinate. The assumption of homolytic bond dissociation was made because of the temperature at which this decomposition occurs. These temperatures are in-line with typical combustion reaction temperatures, and many of these mechanisms follow homolytic dissociation and radical formation pathways, despite being organic chemicals such as methane, iso-octane, cetane, benzene, etc, showing that at high temperatures, the nature of the organic chemistry of fuels has a tendency to shift from heterolytic to homolytic pathways.[1][2][30][31][35][36][37][58][67]

5.1.1 Chain Initiating Reactions

Three new chain initiating reactions have been identified from the high density ReaxFF simulations run using the nitramine combustion force field.[45][46][47] The first of which is the reaction

$$CH_3NO_2 \leftrightarrow \dot{C}H_2NO_2 + \dot{H}$$

where a proton dissociates homolytically from the methyl group of nitromethane. This reaction, of the three chain initiating reactions, is the most prevalent. At high densities, the proton dissociates from the methyl group due to the postulated carbon-hydrogen bond strength reduction caused by the molecular compression that occurs at elevated pressures, coupled with large London

dispersion forces and instantaneous dipoles generated by the highly polar molecules being forced into close proximity with each other. The highly negative nitro group on a nearby molecule tends to repel the electron cloud responsible for maintaining bonding character with the sp^3 hybridized carbon. The nitro group on the dissociating molecule behaves in a similar fashion, forcing the charge density of the carbon-hydrogen bond to re-orient specifically toward the carbon nucleus. One proton in particular experienced this effect stronger than the other two, being aligned in plane with the nitro group on the opposite end of the same molecule. This reduction in bond strength allows for complete bond dissociation, and the highly diffuse and energetic proton is free to rapidly leave the local reaction site, likely preventing the reverse reaction from proceeding fast enough to balance the forward.

The second initiating reaction that occurs is shown below.

$$CH_3NO_2 \leftrightarrow CH_3NO + \dot{O}$$

In this reaction, the nitromethane monopropellant dissociates such that an oxygen atom leaves the sp^2 hybridized nitrogen atom. For this to occur, the resonance in the nitro group must be destabilized, leading to the formation of nitrosomethane. Nitrosomethane is thermodynamically unstable compared to its structural isomer, formaldoxime, but is the first analogue of nitromethane that will occur from this dissociation. Nearly immediately after this dissociation occurs, this species is then stabilized as the remaining oxygen atom can strip a proton from the methyl group and undergo intramolecular rearrangement,

leading to the formation of formaldoxime, the aldoxime of formaldehyde. This rearrangement is shown in the figure below.

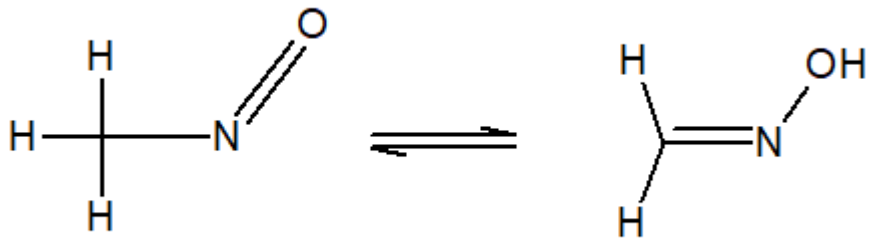

Figure Twelve: Nitrosomethane - Formaldoxime Structural Isomerization Reaction

This reaction has been presented as an initiating step in the past, and has been subject to controversy amongst several previous publications. The most common detractor of this reaction is that it has a higher activation energy than the traditional carbon-nitrogen bond scission, but this simply makes reaction less likely to occur in statistical probability; this does not mean that it will not occur. Like the first proposed reaction, high density may cause both intermolecular and intramolecular effects that could reduce the overall energy barrier, making it more relevant at elevated pressure. Aerojet also proposed an alternate mechanism through which this reaction can occur, where an oxygen atom on the nitro group can create a hydrogen bond with a proton on the methyl group, stabilizing the transition state.[25] Then, through a reduced energy barrier pathway, formaldoxime can be made immediately, bypassing the formation of nitrosomethane, and losing an oxygen simultaneously.

The third and final initiating reaction to be added to the traditional thermal decomposition mechanism is akin to the second reaction, but follows the Aerojet proposed mechanism rather explicitly.[25] Steric strain and hindrance of

the nitro group and methyl group to cleanly rotate about the carbon-nitrogen bond axis activates the molecule. This activation leads to the formation of a bond between an oxygen on the nitro group and a proton on the methyl group. At this point, this reaction diverges from the Aerojet scheme; these instead combine and leave the nitromethane molecule in the form of a hydroxyl radical. Despite going through a comparably low-energy transition state than the second reaction, the hydroxyl elimination reaction directly from nitromethane is the least likely to occur since the energy required to cleave both the carbon-hydrogen and resonance stabilized nitrogen-oxygen makes this reaction less probable. This reaction proceeds as

$$CH_3NO_2 \leftrightarrow H_2CN\dot{O} + \dot{O}H$$

In a two-step process, an intramolecular rearrangement occurs where the nitro group attracts a proton from the methyl group, and a hydroxyl radical fully dissociates from the molecule. Activation energies for the first two initiation reactions were calculated from DFT based calculation at the 6-311+G* level, described above. The third reaction was estimated from tabulated homolytic bond dissociation energies, with adjustments to these values made based off Mayer bond orders from DFT results, in order to more closely approximate reality. Reaction three has an activation energy equivalent to the activation energy of reaction one, with the additional barrier energy associated with the destabilization of the nitro group's electronic resonance. Resonance and electron delocalization created an energetic stability that is apparent in the DFT population analysis, manifesting itself as an N-O average bond order greater than

1.5, which would numerically be the average bond order based on the two resonance contributors.[38] There is also a small bond order present between the two oxygen atoms, a contributing factor to the delocalization stability. The stability energy is twelve kilocalories per mole, and the total activation energy is 117.32 kilocalories per mole.[38][64] Activation energies were calculated similarly for the remainder of the reactions discussed.[38][64]

5.1.2 Chain Branching Reactions

Chain branching reactions occur post-initiation, and are elementary steps that lead to an increased concentration of radicals, and accelerating the overall rate of reaction. Four chain branching reactions were distilled from the ReaxFF data, three of which tend to happen in chronological order through the reaction set. The first is an activation of the initial nitromethane fuel by protonation via hydrogen peroxide. The peroxide binds to the nitromethane molecule by hydrogen bonding, and strips a proton, releasing as a more reactive hydroperoxyl radical. The second chain branching reaction continues from here, when the now protonated nitromethane dissociates, becoming nitrosomethane and a hydroxyl radical. Nitrosomethane, being thermodynamically unstable, rearranges itself to formaldoxime. Lastly, in the final chain branching reaction that was examined, formaldoxime decomposes into a formaldoxyl radical and a proton. These three reactions are summarized as follows

$$CH_3NO_2 + H_2O_2 \leftrightarrow CH_3NOOH + H\dot{O}_2$$

$$CH_3NOOH \leftrightarrow CH_3NO + O\dot{H}$$

$$CH_3NO \leftrightarrow H_2CNO + \dot{H}$$

The fourth reaction is a HONO elimination pathway for a protonated nitromethyl radical. This is the main relevant consumption pathway for this species. In a direct electron shift, HONO dissociates from CH_2NOOH because if its electronic stability, coupled with a reduction in the spin state of CH_2. The single unpaired electron on the CH_2 side of the atom can move in toward the bonded side of the carbon and couple to form singlet carbene, allowing HONO to exist on its own in an unbound state.

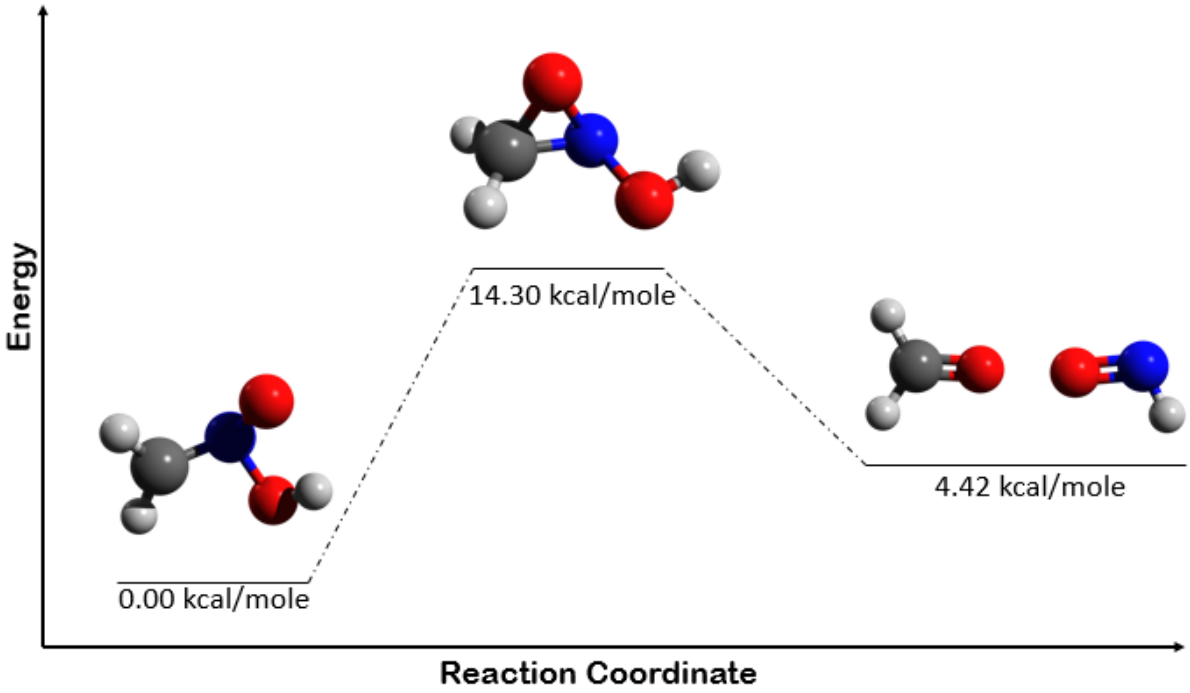

Figure Thirteen: Reaction Map of CH_2NOOH Rearrangement Reaction

Another viable CH_2NOOH dissociation reaction was investigated as well, the rearrangement reaction akin to methyl-nitrite rearrangement in nitromethane. The nitro-group rocking mode on this molecule can potentially lead to a transition state in which the radical oxygen and radical carbon centers bond and form a three center (C-N-O) ring species. This path lays the

groundwork for dissociation; the electrons between the carbon-nitrogen bond swing in and back toward the oxygen atom, creating formaldehyde and HNO. The reaction map, as calculated from DFT/B3LYP level calculation using the 6-311+G* basis set, are shown above. The activation energy for this reaction is far lower than the HONO elimination pathway, but the HONO elimination pathway is predicted to have a higher pre-exponential factor because of its mechanistic simplicity. Under the assumption that these effects cancel each other out, the reaction data for nitromethane dissociation to a methyl group and nitric oxide was used for the reaction added to the dataset in Chemkin. The activation energy is approximately half way between the activation energy of the HONO elimination reaction of CH_2NOOH and its rearrangement dissociation, yielding a representative consumption rate of both reactions. This was used with the dissociation reaction to CH_2 and HONO because of its predicted overall rate than rearrangement. These assumptions are also made in tandem with the fact that CH_2NOOH production in the flame is minor, so its influence on the flame structure is insignificant as well. The hydroxyl dissociation reaction observed in the ReaxFF results was not included here because the bond dissociation energy of that reaction was 45.71 kilocalories per mole, as calculated by DFT at the B3LYP level.[38] This energy was higher than both other reactions surveyed and was, therefore, explicitly excluded.

The fifth chain branching reaction involves the interaction of a hydroxyl radical with nitromethane. In this reaction, the hydroxyl radical binds to the nitro-group side of nitromethane. This creates an ersatz six-membered ring as

primary transition state, in which the oxygen on the hydroxyl bonds to an oxygen in the nitro group, and the hydroxyl radical's proton hydrogen bonds to the other. From this ring, a diatomic oxygen molecule forms, and the remaining proton leaves simultaneously. The nitrosomethane left behind rapidly begins tautomerization to formaldoxime via intramolecular proton shift. This proton is deflected by either the hydroxyl proton that leaves the reaction or the diatomic oxygen molecule. O_2 will also pull this proton away via hydrogen bonding interaction as it leaves. This reaction is written as

$$CH_3NO_2 + \dot{O}H \rightarrow 2\dot{H} + O_2 + H_2CNO$$

5.1.3 Chain Propagating Reactions

Chain propagating reactions, like chain branching reactions, are post-initiation elementary reaction steps that progress a combustion reaction through the formation of radicals. Unlike chain branching reactions though, chain propagating reactions do not increase the net concentration of radicals, they only stand to progressively transition reactant-like radicals toward more product-like radicals, or other radical species that then participate in chain branching reaction sets. Four reactions in this set have been identified as chain propagating reactions. The first two are defined as

$$CH_3NO_2 + \dot{H} \leftrightarrow CH_3NOOH$$

$$CH_3NO_2 + H_2O \leftrightarrow CH_3NO + H_2O_2$$

The first reaction begins to occur when the weakly nucleophilic hydrogen radical is attracted to the partially positive nitrogen atom on the nitromethane.

Once the hydrogen atom moves within close proximity, hydrogen bonding to the oxygen atoms as well as a radical-pi interaction with the conjugated nitro group lowers the barrier energy for the forward reaction and allows the proton to bond with one of the oxygen atoms, forming a protonated nitromethane molecule. In the second reaction, a common theme amongst nitramine and nitrate fuels can be seen; water sensitizes the reaction. The water molecule approaches nitromethane perpendicular to the carbon-nitrogen bond axis. Two hydrogen bonds form, one between a proton on the water molecule and an oxygen on the nitromethane, and the other between the oxygen atom in the water molecule and a proton on the nitromethane's methyl group. From this six center transition state, the bound proton from the water molecule protonates the nitro group in the same manner as the first reaction, while the rest of the water molecule remains bound to the methyl group as a hydroxyl radical. This hydroxyl radical then approaches the protonated side of the nitro group, and leaves the nitromethane molecule as peroxide, leaving nitrosomethane behind. This rapidly rearranges intramolecularly to formaldoxime, creating a more thermodynamically stable intermediate species for the global reaction.

The next chain propagating reaction is a proton abstraction reaction that occurs between formaldoxime and a hydroperoxyl radical. When the two molecules come within close proximity, a four center transition state forms between the alcohol group of the formaldoxime and the hydrogen and oxygen on the hydroperoxyl radical. A proton is then transferred to the hydroperoxyl from formaldoxime, completing the formation of hydrogen peroxide and formaldoxyl

radical. The radical product of this reaction is consumed as a common intermediate in the base nitromethane decomposition reaction set. Therefore, further reactions defining the consumption of this species are not required and are expected to follow the base reaction set. This reaction is shown below.

$$CH_3NO + H\dot{O}_2 \leftrightarrow H_2CNO + H_2O_2$$

The last of the chain propagating reactions is a multistep decomposition of protonated nitromethane. In this reaction, an acidic proton from the methyl group of the molecule dissociates, changing the hybridization of the carbon atom to sp^2 geometry. Simultaneously, the hydroxyl group dissociates from the nitrogen atom in this molecule via homolysis due to electronic destabilization. Similar to the previous reaction, this leads to the formation of a formaldoxyl radical, tying this reaction into the rest of the existing reaction set smoothly. This reaction was distinguished from the separate CH_2NOOH consumption reaction because of the relative lifetime of CH_2NOOH in this reaction.

5.1.4 Chain Terminating Reactions

Chain terminating steps directly lead to final products, signifying the end of the global reaction. This reaction set was specifically developed as an appendage to the baseline in order to adjust the initiation. By its nature, it includes minimal reactions that could be considered chain terminating. The reactions discussed in this section were chosen as the reactions signifying the end of the initiation chemistry. From this, three reactions were identified. These final three reactions are as follows

$$CH_3NO \leftrightarrow H_2CNO + \dot{H}$$

$$CH_2NO_2 + \dot{O}H \rightarrow H_2CNO + \dot{H} + O_2$$

$$CH_3NO \rightarrow CH_2N + \dot{O}H$$

5.2 Added Species

A couple of species needed to be added to the current mechanism in order to properly integrate the new reaction set defined herein. These species include the protonated nitromethane molecule and the protonated nitromethyl radical. These two molecules were not previously included in the reaction sets. In order to simplify the integration into Chemkin, transport parameters for nitromethane and the nitromethyl radical were used for the protonated analogs of each species, since the proton itself is relatively small and should not dramatically affect transport and diffusivity data for these two species, especially since they are expected to be short lived within the flame. A majority of the reactions defined above are given as forward only reactions in Chemkin, so the thermodynamics used in calculating the reverse reaction rates are of little importance. Calculated energies from DFT of the added species are very similar to nitromethane, so the thermodynamic parameters for nitromethane were used to model these species. This has little impact on the flame calculation itself because the final flame temperature is a function of reaction enthalpy, which itself is a state function and is unaffected by the properties of these early intermediates. The early reaction steps also have minor heat addition relative to later components of the global

reaction, and the added reactions occur in tandem with other established reactions, so the overall effect of assuming nitromethane thermodynamic properties for the added analogous species is insignificant for this qualitative analysis.

A series of reactions involving the formation of methyl hydroperoxide and its corresponding radicals were also included. These species showed up in the ReaxFF simulation, and have also been observed in other combustion reactions, such as the Lawrence Livermore National Labs (LLNL) trinitro-toluene (TNT) mechanism.[37] Some of the reactions found in the LLNL TNT mechanism were adopted for use in the Chemkin mechanism because they incorporated other reactions observed in the molecular dynamics not included in the baseline Chemkin mechanism. These reactions do not pertain directly to the initiation mechanism being investigated, but were included for completeness. The significance of these reactions is that, according to the ReaxFF, the methyl peroxyl radical is the main former of singlet methylene ($CH_2(S)$) in nitromethane combustion, which contributes to the small molecule chemistry of the flame as well as the carbon fragment recombination. Fragment recombination is the only potential pathway for polycyclic aromatic hydrocarbon and soot formation.[65][66][67][68][37]

5.3 Observations and Implications

Much of this reaction set, when added to the baseline reaction mechanism, shows flame structure similar to the decomposition of other monopropellants. The baseline mechanism, though accurate at predicting low pressure structure

and flame speed, and plausibly accurate at predicting flame thickness in the current state, does not aptly depict the complex and staged flame structure reminiscent of nitromethane, and similar to that of double base gun propellants. Speculation about the possibility of this hydrogen abstraction initiation mechanism has been unfavorable, but also incorrect in its basis. Hydrogen abstraction does not dominate entirely over carbon-nitrogen bond scission, the two initiation mechanisms occur side by side. It is also most likely to occur through homolytic bond dissociation pathways, rather than the previously published heterolysis pathways. Heterolytic bond dissociation, though common in low temperature organic chemistry and synthesis, is seldom seen in the high temperature environments that combustion mechanisms occur at. Lastly, though true that carbon-nitrogen bond scission is apparently more thermodynamically favorable, this does not mean that it occurs explicitly and uniquely.

C_2 chemistry has implications in this reaction set despite the fact that the initial fuel has only a single carbon. Methyl fragment recombination has potential to occur just the same as other combustion mechanisms such as the GRI Mech for natural gas combustion. This recombination sets the frame for sooting in nitromethane flames. C_2 chemistry is predominant in this, because it's far less likely that C_3 or higher chemistry, such as that of benzene rings, is going to happen in concentrations of any appreciable statistical significance since there is little free carbon to undergo recombination and there are many other consumption pathways that can occur in tandem with carbon-chain recombination. Acetylene is the main contributor to soot then, and this

mechanism is discussed further in chapter six.[65][66][67][68][37] The other place C_2 chemistry has potential to become important is in accelerating the consumption rate of nitromethane post-initiation. If a methyl radical recombines with a nitromethyl radical to create nitroethane, it changes the dynamics of the carbon-nitrogen bond. The molecule becomes larger in collisional cross section, making third body interactions significantly more likely. It also has increased steric strain in the rotational conformers of the molecule, and the carbon-nitrogen bond strength is changed. According to DFT level calculation, the carbon-nitrogen homolytic bond dissociation energy is 58.47 kilocalories per mole for nitroethane, as opposed to the 60.65 kilocalories per mole for the same calculation on nitromethane.[38] This indicates that the reaction will be faster than the analogous reaction for nitromethane, and thusly could accelerate the consumption rate of nitromethane with increasing methyl radical concentration.

CHAPTER SIX

Soot Formation and Additional Carbon Chemistry

Soot formation is a facet of combustion engineering and research that is has been studied in the interest of topics such as diesel combustion and TNT soot formation, but remains an area less highly studied than other areas in combustion, such as flame instabilities, turbulent flame structure and stretch, and combustion and decomposition mechanisms. In the practical use of nitromethane, the fuel is typically burned in an aerobic environment. This leads to a non-sooting flame. Nitromethane as an oxygenated fuel can reach a much more complete final combustion in service and operation in an aerobic environment. As a monopropellant, however, nitromethane undergoes a fuel rich thermal decomposition, yielding a much higher potential for soot formation due to incomplete combustion. In order to study this, some modifications need made to the nitromethane mechanism being used, and a soot formation mechanism needs identified for use in Chemkin.

Soot is known to form inherently from the chemistry of aromatic hydrocarbons and acetylene.[65][66][67][68][37] The acetylene-based mechanism begins with the deprotonation of acetylene, leading to an HC_2 radical. This radical then undergoes recombination with either another HC_2 radical or a C_2 molecule. Similar to chain polymerization, this reaction set continues until termination, leading to a series of molecules of the geometry $C_{2n}H_2$.[65][66][67][68][37] The deprotonated acetylene can also recombine with methylene and form propargyl (C_3H_3). This species is the first and most prevalent in the development of benzene

in the post flame region. Once benzene has formed, the path to polycyclic aromatic hydrocarbon (PAH) formation is relatively direct. These PAH compounds are ultimately responsible for soot formation; being of high molecular weight and carbon content, PAH compounds tend to condense out of the gas phase as particulate matter.[65][66][67][68][37]

The necessity of higher order carbon compounds in order to study soot formation in nitromethane flames requires the presence of these reactions. The baseline reaction selected for this study, though accurate and modern in many other aspects, is devoid of C_2 and higher order species chemistry. C_2 chemistry has been included in nitromethane thermal decomposition mechanisms since the beginning of its study, as noted in the literature review section of this thesis. The findings of this thesis do not determine why carbon chemistry beyond C_1 was excluded from the baseline mechanism of Melius, and later adapted by Boyer, but it was likely considered auxiliary since those mechanisms were not used originally to investigate soot, and carbon chemistry beyond C_1 does not accumulate appreciably within the flame, even at supercritical pressures relevant in this study. Reactions for this higher order carbon chemistry were taken from the GRIMech 3.0,[58] inclusive of C_2 chemistry only. C_3 chemistry was determined to occur at such low concentrations that it was unclear whether it could be considered reliable or within the error of the software and calculation. These added reactions include formation of ethane, ethene, acetylene, ketene, acetaldehyde, and other more complex C_2 species that would aid in tying the results of the flame calculation to the post flame region calculation using the

sooting mechanism. Nitroethane was excluded from the reaction set. The carbon-nitrogen bond fission energy of nitroethane, though lower than nitromethane's, is not vastly different, and the species is not expected to develop substantially; in the event of methyl – nitromethyl collision, dissociation would likely occur either in the reverse direction, or as nitromethane and carbene, rather than as nitrogen dioxide and an ethyl radical or as C_2H_5O and nitric oxide. The complexity of additional reaction sets involving nitroethane was therefore discarded under the presumption of minimal impact. It was noted above that nitroethane has the potential to accelerate the reaction under high methyl radical concentration, and would possibly be of greater interest in blended fuels of nitromethane.

CHAPTER SEVEN

Chemkin Reaction Modeling

7.1 Baseline Results

ANSYS Chemkin 19.2 was used to test the reaction set and examine the effect of the added reactions proposed in this paper on properties such as heat release profile, flame temperature, ignition delay time, and speciation.[69] In order to do so, baseline results need to be developed. The reaction mechanism assembled by Boyer was used as the initial dataset that was used to improve upon.[1] This reaction set utilizes data from Melius and Glarborg's nitromethane reactions,[2][30] Yetter's RDX mechanism,[31] and some of Anderson's dark zone kinetics.[35] This mechanism was run in the closed reactor solver in Chemkin, giving data mainly in the temporal domain. Due to time limitations and difficulty getting the software to effectively and reliably converge on a solution, laminar flame speed data was obtained sparsely, and flame structure in the spatial domain was not extensively examined.

Ignition delay baseline results were set using the mechanism of Boyer et al. in the closed reactor simulator.[1][69] This simulation showed a long delay time and a very one-dimensional development in the flame. The mechanism was developed and optimized for flame speed and flame structure in the spatial domain, and these results were also acquired. Though important for comparative purposes, these results are not presented and discussed here in detail. It is the author's impression that omitting these results is preferable in the interest of

maintaining clarity; the spatial and temporal results are not directly comparable and will lead to reader confusion if a comparative attempt is made.

All simulations were performed at an initial temperature of 800 Kelvin unless otherwise specified. This initial temperature was selected because it follows along with the ReaxFF simulations run in the first half of this research. 2500 psi is very near the lowest pressure that full supercritical burning has been observed by Boyer and Derk,[1][24] so much of the preliminary simulations were run at this pressure. This cuts down on the time needed to iterate on the mechanism and troubleshoot, as well as expanding the flame in the time-domain, making any otherwise compressed and hidden anomalies in the dataset apparent. Once the troubleshooting phase of the initial Chemkin simulations was complete, pressure was increased to 10,000 psi.

7.2 New Mechanism Results

The final appended mechanism used in Chemkin includes the reaction set described in chapter five, but utilizes activation energies and pre-exponential factors assembled from surveying the reaction mechanisms of Anderson,[35][36] Glarborg,[30] Yetter,[31] Pitz, and Westbrook.[37] Dean and Bozzelli's chapter in Gardiner Jr's Gas Phase Combustion Chemistry text was also referenced.[70] Some preliminary sensitivity analysis was performed on these reactions, and the dataset that was concluded on was used because it depicts a clear flame structure that can be discussed easily as a set of qualitative results. Some reactions showed high sensitivity to variations in pre-exponential factor, such that moving two orders of magnitude faster would result in a failure to converge and present a

solution. The dataset used did not deviate far from the reaction rates of analogous reactions in the surveyed combustion mechanisms, converged smoothly, and gave clear results that are easy to qualitatively discuss.

The temperature profile shows very interesting results for the flame structure. It can be broken down into four different regions; primary ignition, secondary ignition, a plateau, and tertiary ignition. These regions can each be discussed on the basis of their chemistry alone. Nitromethane is well studied by virtue of the fact that it's the simplest nitro-hydrocarbon, and its chemistry is expected to give insight into the chemical progression of more complex species. The flame structure described in these results gives an example of how complex nitromethane combustion can be on its own.

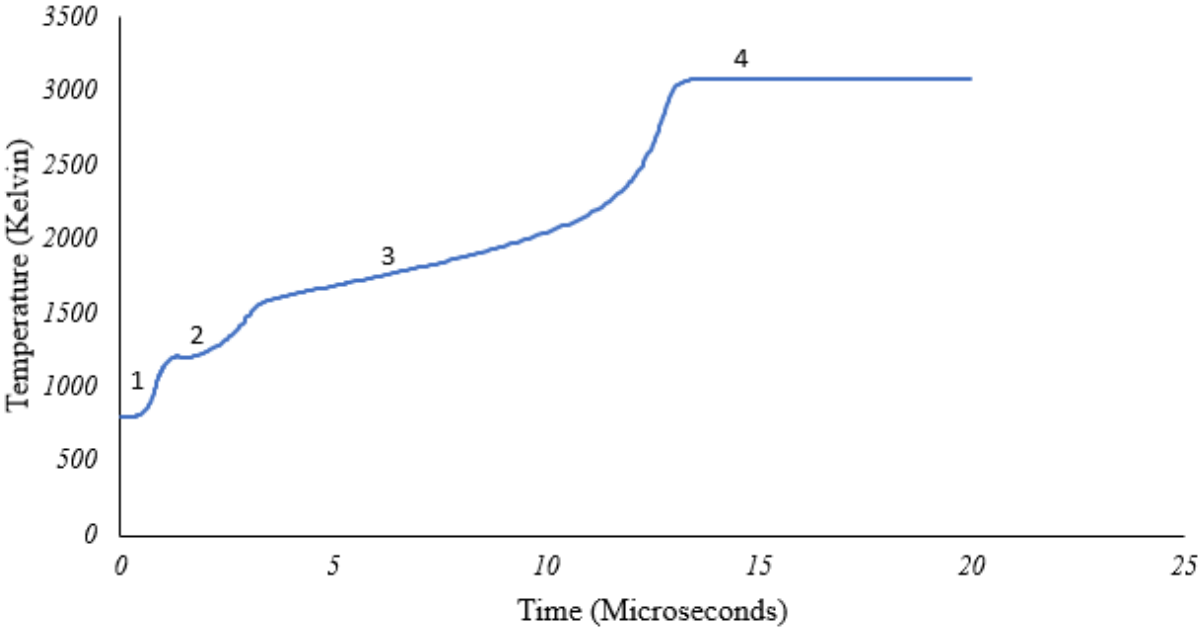

Figure Fourteen: Temperature Profile of 10,000 PSI Nitromethane Flame (Chemkin)

The primary and secondary ignition events are both low temperature combustion events, yielding minimal heat release compared to the final ignition

event. The same nitromethane flame case run in Chemkin using the baseline mechanism shows long ignition delay time, with a thin flame that's hardly resolvable in the software. The flame event occurs so fast relative to the ignition delay time that it appears to be a nearly spontaneous. With this appended mechanism, ignition delay time is brought to a very short value, similar in time and structure to the analytical results Melius had originally published on.[2] The primary and secondary ignition events occur because of the hydrogen abstraction initiation mechanism and the carbon-nitrogen bond fission initiation mechanisms, respectively. Once the hydrogen abstraction initiation begins to occur via homolytic dissociation pathways, and minor reactions begin to occur, the number density of molecules and fragments in the system increases, accelerating the onset of carbon-nitrogen scission.

From here, the thermal plateau region of the flame develops. It's important to note that this region is highly sensitive to pressure, and tends to follow the same mechanistic pathways that are seen in a dark zone behind a nitramine or nitrocellulose (smokeless gun powder) flame.[35] Highly diffuse, low level species move freely through this region of the flame, interacting and interchanging toward product-like intermediate species. At 5000 psi, this region in the flame had a much flatter and longer temperature trace than at 10,000 psi. As pressure increases from 10,000 psi to 30,000 psi, this region condenses and the temperature trace converges on a linearly increasing characteristic. It is known that dark zone breakdown has a massive influence on overall burn rate in other propellants, as was discussed by Anderson in his aforementioned paper on

dark zone kinetics.[35] A similar effect is seen here, where the longest part of the flame, and one of the more pressure sensitive, is ultimately going to have the strongest effect on flame speed.

Figure fifteen shows the speciation profile of the newly added initiation mechanism

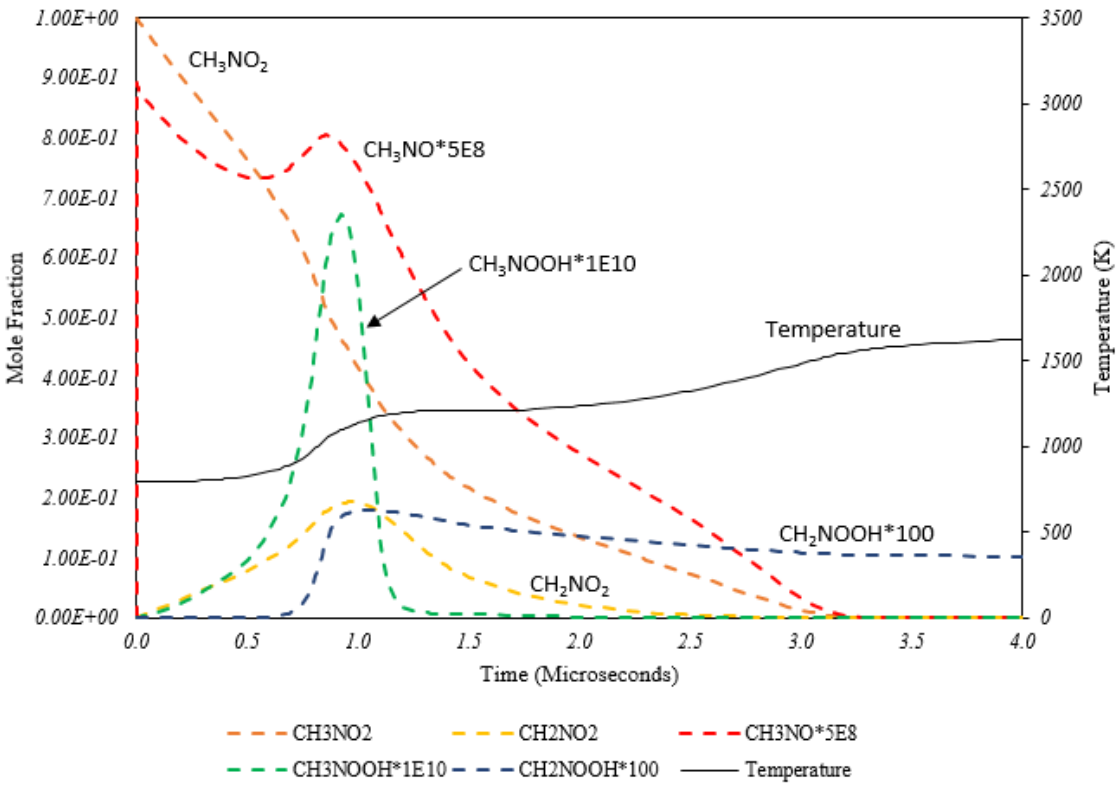

Figure Fifteen: Speciation of New Initiation Mechanism from Chemkin at 10,000 PSI

at this pressure, with temperature plotted on the secondary abscissa. As mentioned previously, the flame profile of supercritical nitromethane exhibits a similar characteristic to a double base gun propellant.[35] An initial low temperature ignition occurs, caused by the initial decomposition of propellant to activated intermediate species. During this first stage ignition, CH_2NO_2 forms

first as nitromethane is consumed. Near the apex of CH_2NO_2 concentration, CH_2NOOH begins to form. CH_2NO_2 recombines with hydrogen atoms and generates CH_2NOOH. Similarly, trace amounts of CH_3NOOH forms through nitromethane proton abstraction, and is consumed in the generation of CH_3NO.

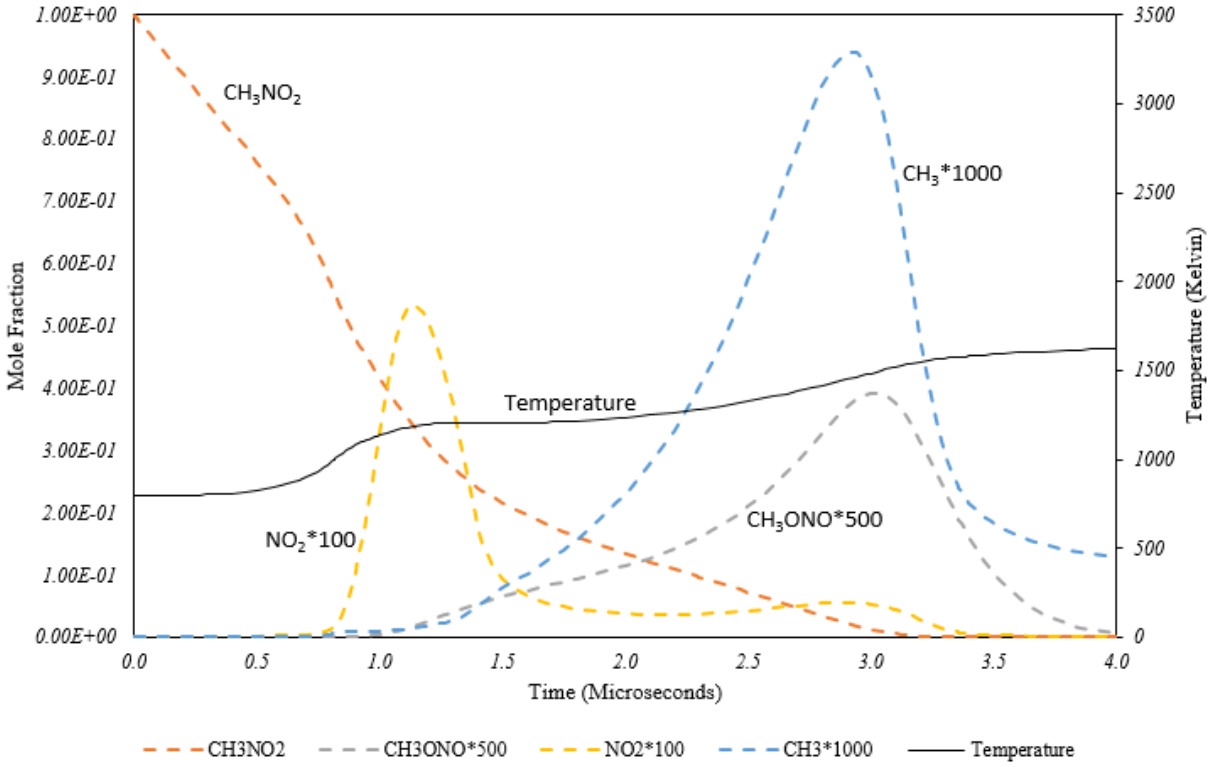

Figure Sixteen: Speciation of Carbon-Nitrogen Bond Fission from Chemkin at 10,000 PSI

After the second low temperature initiation, the flame enters into a plateau in temperature, the longest duration event in the structure of the flame. Dark zone chemistry is particularly prevalent here; small diffuse molecules undergoing rearrangement and substitution reactions with low thermal signature dominate this segment of the flame.[35] The chemistry can be broken down into nitrogen chemistry, carbon chemistry, and cyanide chemistry. Nitrogen chemistry takes

the form of amine and amide speciation in the intermediate flame, with nitrogen oxide chemistry being more of interest in the beginning and end points of the flame. Events occur slowly in this region, concentrating product precursors until the reaction rates begin to take off exponentially and form final products.

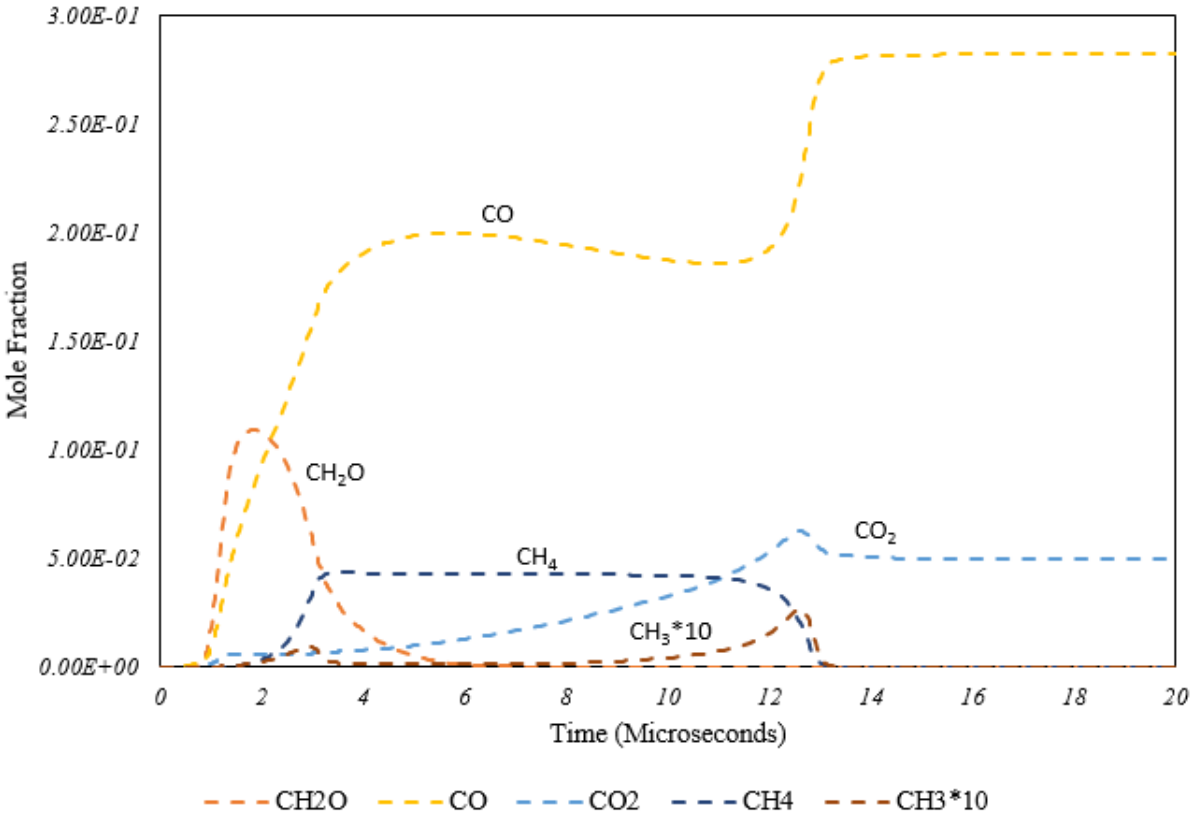

Figure Seventeen: Hydrocarbon Oxidation Species from Chemkin at 10,000 PSI

The hydrocarbon oxidation process in the nitromethane flame is rather direct, initially generating formaldehyde and carbon dioxide. Small amounts of CH_3O are formed from methyl nitrite rearrangement and dissociation, but these molecules are not long lived and contribute quickly to the formation of formaldehyde. At the end of the secondary initiation, formaldehyde is converted to methane and carbon monoxide simultaneously. In the dark zone, methane slowly decays to methyl radicals and atomic hydrogen. Carbon monoxide also

oxidizes further in this region, generating carbon dioxide. At the end of the dark zone, methane decays rapidly, as do the methyl radicals that form. A portion of the formed carbon dioxide reduces, and the concentration of carbon monoxide increases sharply, forming a final equilibrium of monoxide and dioxide oxidation states.

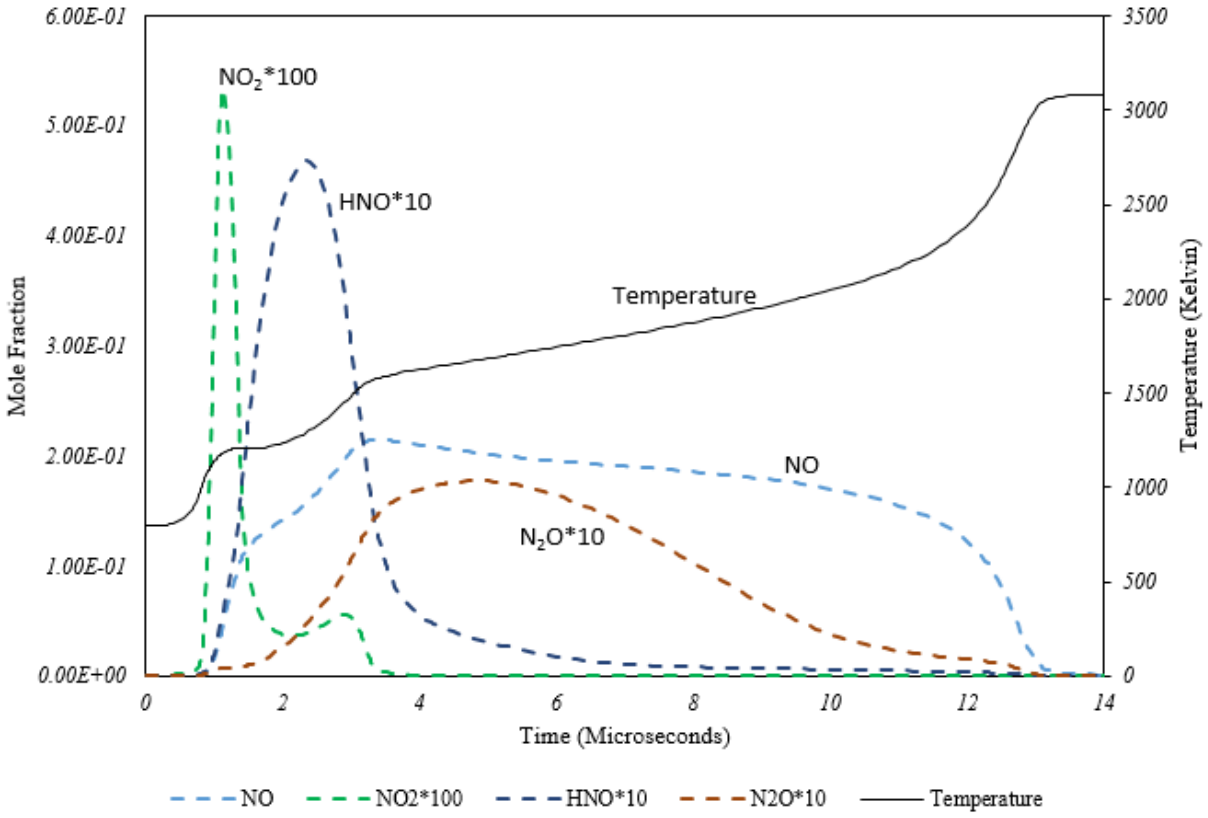

Figure Eighteen: Nitrogen Oxide Speciation from Chemkin at 10,000 PSI

Nitrogen oxide formation in the flame is critically important in the staged flame structure that forms, particularly in the dark zone region. Oxide formation begins primarily after the primary initiation step, then carbon-nitrogen bond fission begins to occur. Nitrogen dioxide concentration peaks rapidly at the end of primary initiation, and decays nearly as promptly. Nitroxyl forms from the decay of nitrogen dioxide, as does nitric oxide. Nitroxyl dissociates toward the

end of secondary ignition, increasing the concentration of nitric oxide further, and forming nitrous oxide which is mainly active in the dark zone. Nitrous oxide formation continues slowly into the dark zone region, along with the decay of nitroxyl, reaching a peak early into this stage in the flame. Nitrous oxide concentration then begins to deteriorate through the dark zone, along with nitric oxide and cyanide, affording the basis for cyanic and iso-cyanic acid formation.

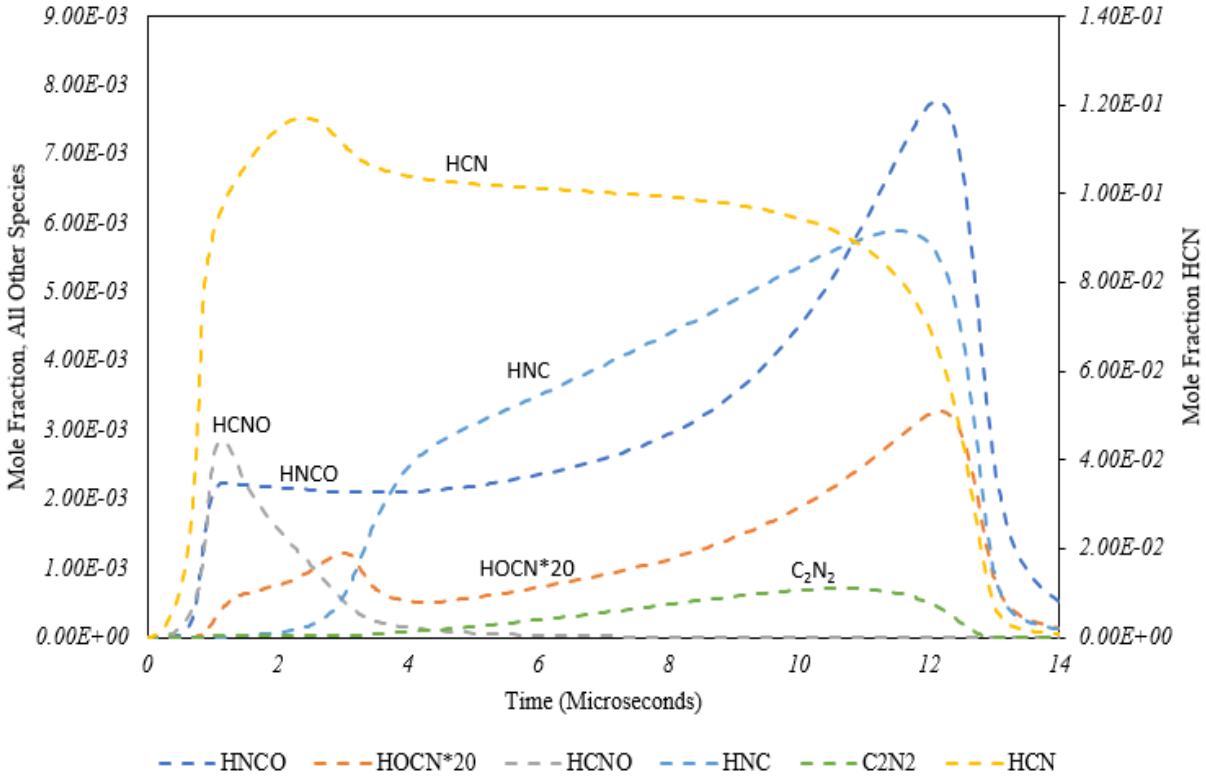

Figure Nineteen: Cyanide Speciation from Chemkin at 10,000 PSI

Figure nineteen shows the formation of cyanide compounds in the flame. It can be seen that these species are highly active throughout the dark zone region. Cyanide forms early in the flame to relatively high concentration. It depreciates slowly through the dark zone, reacting with the nitric and nitrous oxides to form cyanic and iso-cyanic acid. Fulminic acid, the HCNO isomer acid of cyanide, is generated early in the flame during the primary ignition event,

along with cyanide, but decomposes during the secondary initiation event and has essentially disappeared by the dark zone stage of the flame. Along with cyanic and iso-cyanic acid, hydrogen isocyanide (HNC) forms from tautomerization of cyanide. Near the end of the dark zone, cyanide concentration sharply declines as HNCO, HOCN, and HNC concentrations rise accordingly. Cyanogen (C_2N_2) also forms briefly in this region of the flame, before all aforementioned species are rapidly consumed, leading into the termination stage of the flame.

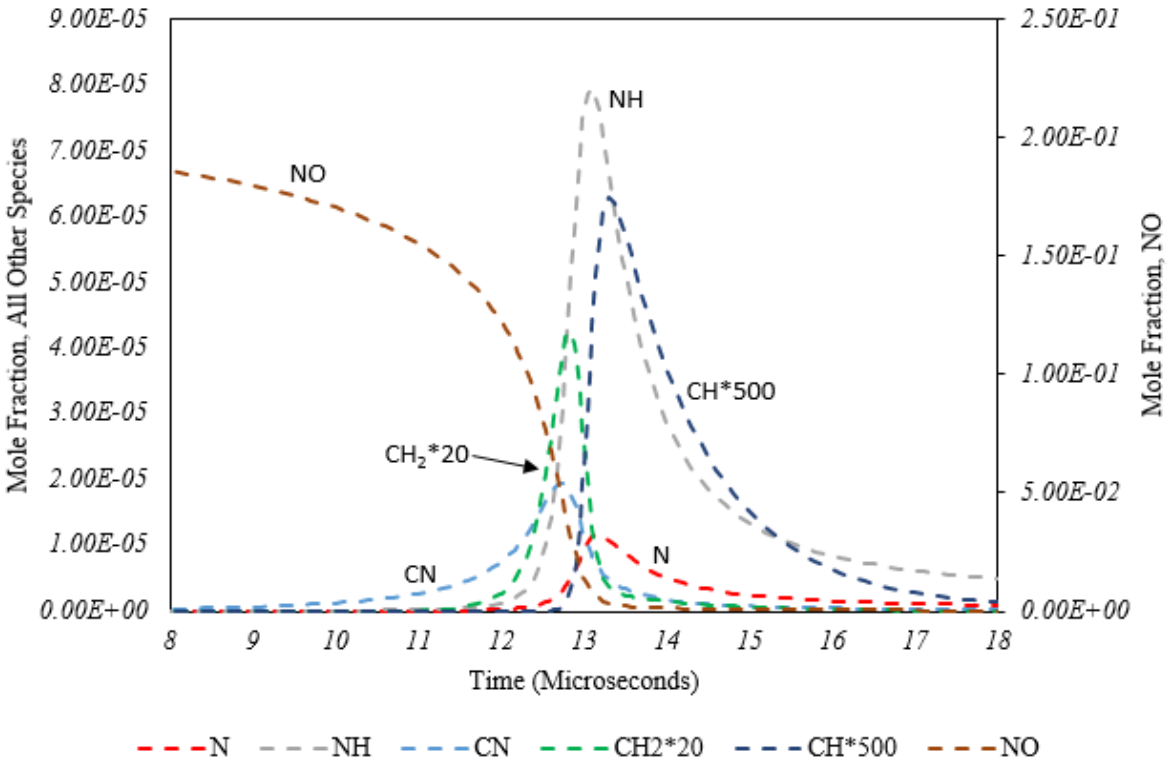

Figure Twenty: Fenimore NO_x Chemistry from Chemkin at 10,000 PSI

Fenimore NO_x chemistry is particularly important in the final stage of the supercritical nitromethane flame structure.[71] Zel'dovich NO_x chemistry was of less importance for two main reasons; temperature was too low to properly observe equilibrium in the Zel'dovich reactions, and the thermal decomposition

reaction here works in the reverse direction of typical aerobic combustion.[72] In this reaction, nitrogen oxides are the reactant species, acting as oxidizers through the flame before forming diatomic nitrogen as a product. Fenimore NO_x is prevalent here because it can proceed more readily at lower temperatures and occurs in series with hydrocarbon oxidation by nitrogen oxides.[71] Figure twenty above shows how the Fenimore NO_x reactions are highly active at the end of the dark zone, leading to flame termination. Nitric oxide concentration degrades rapidly at the end of the dark zone as methylene (CH_2), aminylene (NH) and cyanide (CN) begin to form. Methylene decays to methylidyne (CH), and cyanide decays to form atomic nitrogen. Aminylene persists slightly longer in the flame before decaying toward final products.

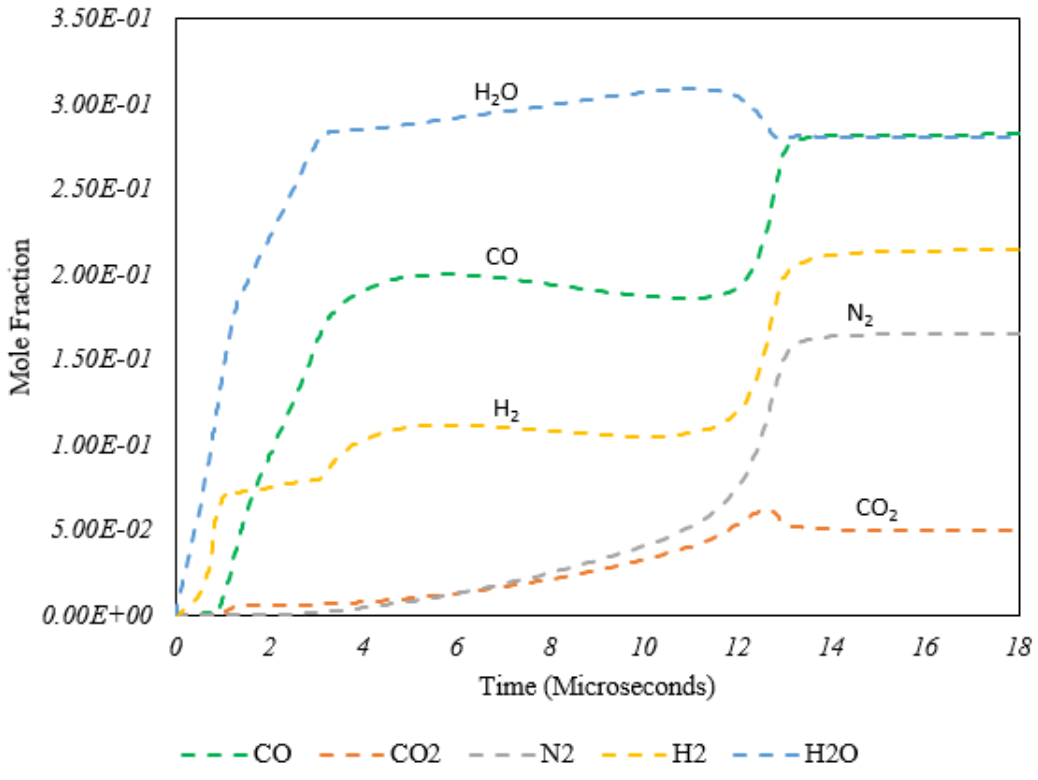

Figure Twenty-One: Final Product Species of Nitromethane from Chemkin at 10,000 PSI

The five main final product species of nitromethane are shown throughout the flame in figure twenty-one. Molecular hydrogen, carbon monoxide, and water are all formed within the primary and secondary initiation stages of the flame. In the dark zone, hydrogen and carbon monoxide are consumed to a minor degree in the formation of intermediate species. At the same time, water concentration increases in the dark zone, and carbon dioxide and diatomic nitrogen are formed. At the end of the dark zone, the concentrations of N_2, CO, and H_2 all sharply increase to their final values. Carbon dioxide increases slightly, and then decreases abruptly to its final value, as does water. Carbon dioxide is reducing and contributing to the final formation of carbon monoxide, and water is acting as an oxidizer for hydrocarbon species in the system and forming H_2 and carbon monoxide. These five species compose 99.3% of the total final products of the nitromethane thermal decomposition at 10,000 psi

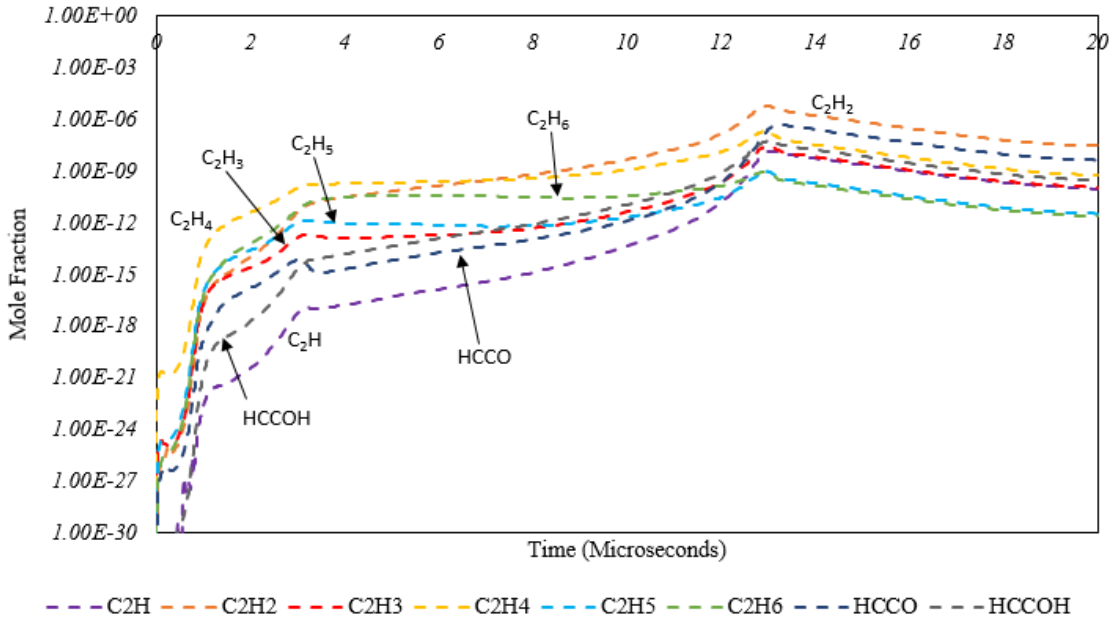

Figure Twenty-Two: C_2 Speciation Added from GRIMech 3.0 to the Nitromethane Flame at 10,000 PSI

According to the work done by Pitz and Westbook at LLNL on the formation of soot in TNT flames,[37] and supported by the work of Howard, Richter, Miller,[66] and Melius,[2] soot precursors developed in the flame are indicative of PAH and soot formation in the post-flame region. These soot precursors include acetylene, vinyl radicals, and unsaturated hydrocarbons. Figure twenty-three shows the soot precursor fraction through the 10,000 psi nitromethane flame.

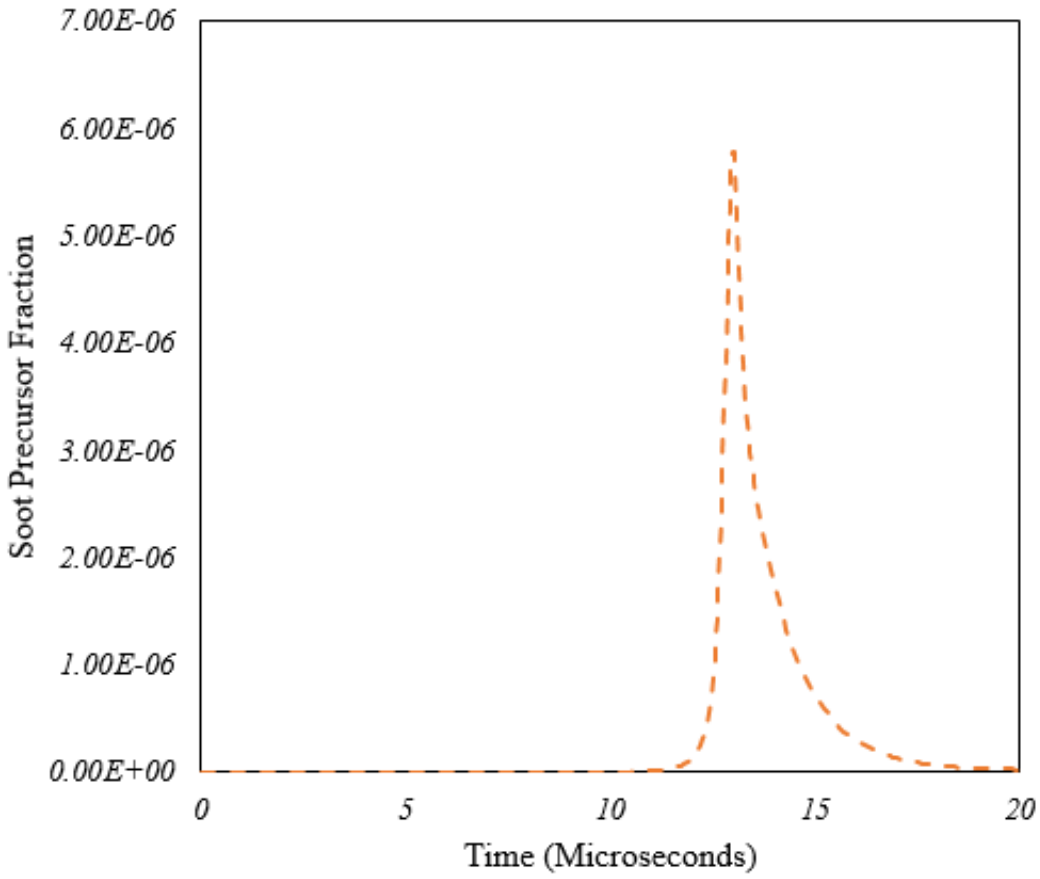

Figure Twenty-Three: Soot Precursor Fraction in the 10,000 PSI Nitromethane Flame from Chemkin

‘ This figure shows that soot precursor fraction peaks immediately at the end of the dark zone region of the flame and is consumed in the generation of final products, particularly CO, CO_2, and H_2. This figure supports evidence of nitromethane flames being low sooting. The mechanism of Richter et al[65][66] was used to further study this in Chemkin. Major product species of the nitromethane

flame were used as input species for the soot mechanism, and a parametric study was performed at 2,500 and 5,000 psi and temperature from 3,500K to 800 K.

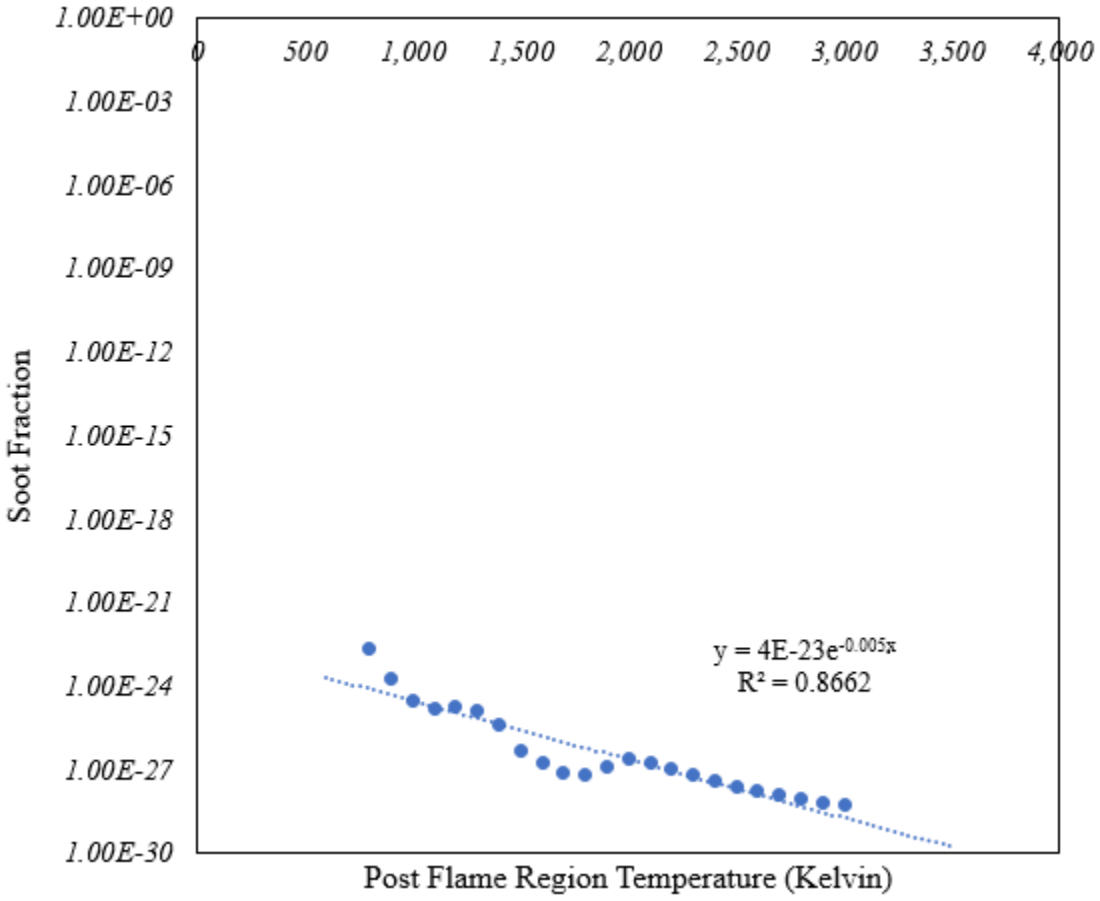

Figure Twenty-Four: Soot Formation at 5000 PSI in the Post Flame Region, Howard Mechanism

Soot fraction in this flame is considered to be the sum of all species present in the mechanism of Richter et al.[65][66] that have a molar mass similar to Indene or heavier. The soot fraction is extremely low, being a percentage of the hydrocarbon content present at the end of the nitromethane flame, showing that nitromethane decomposition is clean, even at high pressure.

As pressure increases, the supercritical nitromethane flame thickness decreases. At 20,000 psi, the time for the nitromethane flame to reach completion reduces from approximately thirteen microseconds at 10,000 psi to seven microseconds. The flame speeds at these pressures, as calculated by the equations given by Derk,[24[are 196 millimeters per second and 313 millimeters per second at 10,000 and 20,000 psi respectively. This makes the stretched, turbulent flame thickness at these pressures on the order of three micrometers at 10,000 psi and two micrometers at 20,000 psi. Figure twenty-five shows the temperature profile at 20,000 psi.

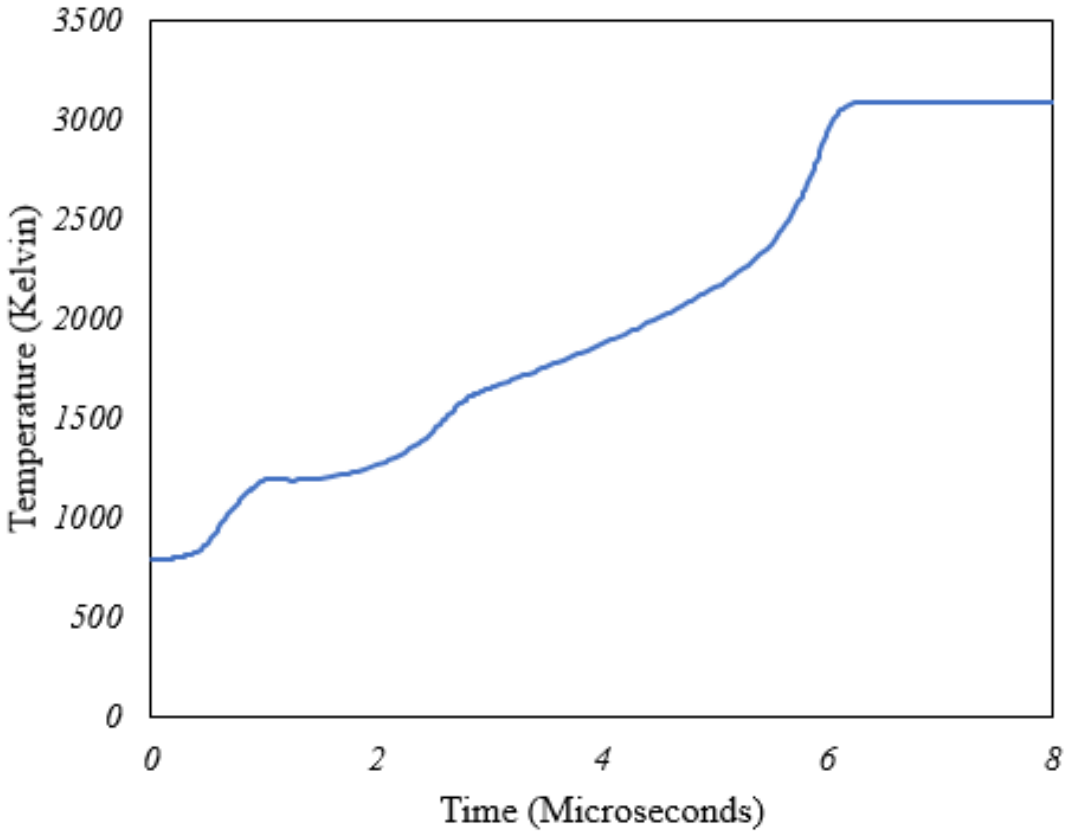

Figure Twenty-Five: Temperature Profile of 20,000 PSI Nitromethane Flame from Chemkin

At 30,000 psi, the time for the flame to terminate reduces to five microseconds. With a calculated turbulent flame speed of 412 millimeters per

second, the stretched turbulent flame thickness at 30,000 psi is two micrometers, the same as the 20,000 psi case. As the pressure increases, the flame speed begins to plateau, as does reaction time and flame thickness. The profile of the flame does change however. The dark zone region becomes less of an isothermal plateau and begins to become a region of constant temperature increase rate. The original staged flame structure present at 10,000 psi fades and converges on a linearly increasing temperature characteristic.

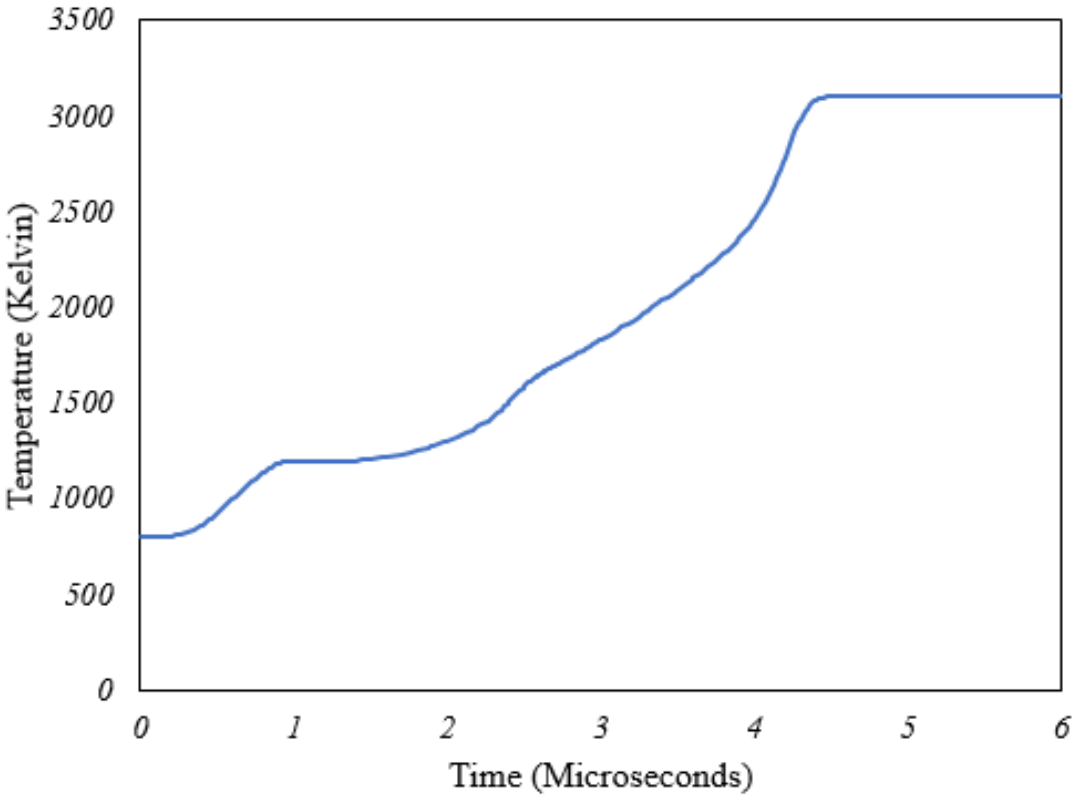

Figure Twenty-Six: Temperature Profile of 30,000 PSI Nitromethane Flame from Chemkin

The isobaric flame temperature of nitromethane is relatively constant, as calculated by Chemkin.[69] The final product species are also essentially constant, and both of these conclusions are as expected. The flame temperature and final product distribution is a state function and essentially dependent only on the

global reaction. The minor product species do change as a function of pressure; this is depicted in figure twenty-seven. As pressure increases, atomic hydrogen, hydroxyl radical, and nitric oxide final concentration decreases. Conversely, as pressure increases, ammonia and hydrogen cyanide final concentration increase.

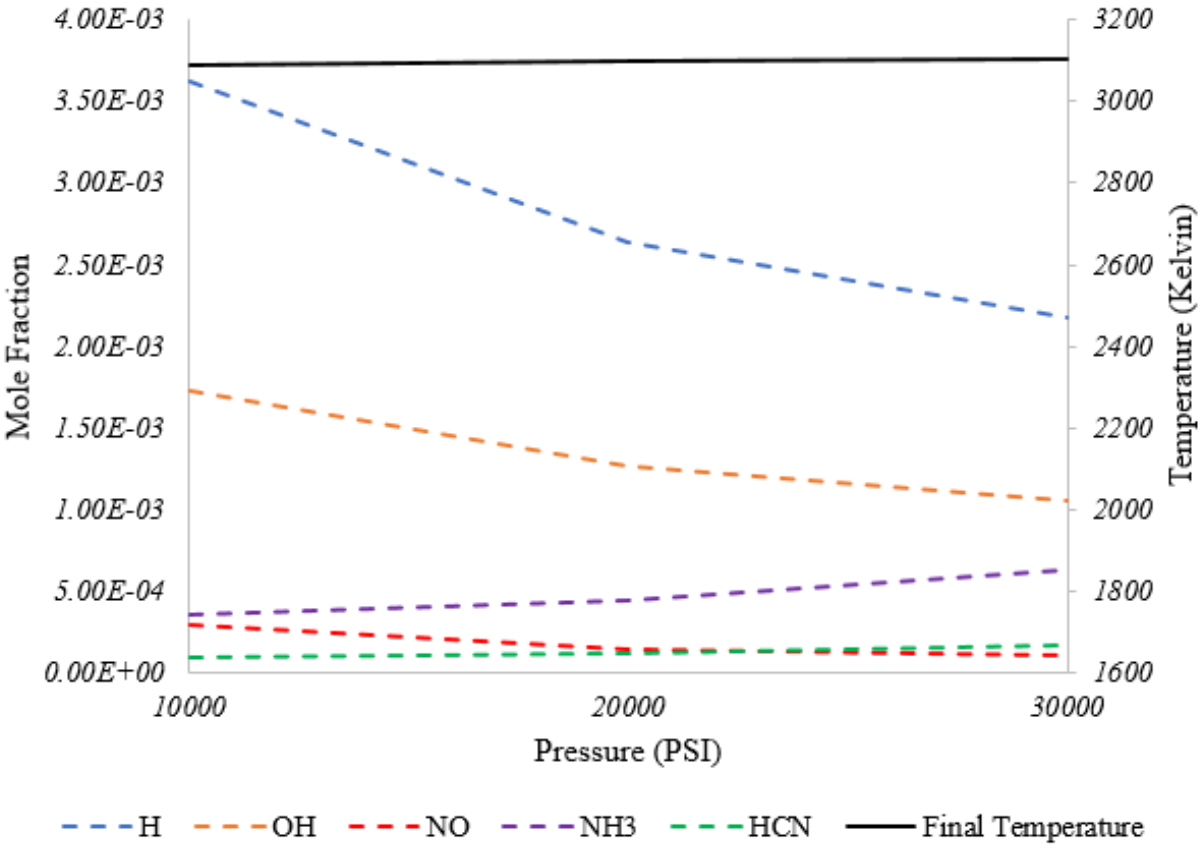

Figure Twenty-Seven: Minor Final Product Species of Nitromethane as a Function of Pressure

7.3 Conclusions

The initiation mechanism presented in this thesis is predicted based on simulations performed in ReaxFF MD simulations. These simulations show that the onset of this initiation occurs at elevated densities in the supercritical state. The initiation mechanism extracted from these data was implemented into an existing decomposition mechanism and examined in ANSYS Chemkin. The

chemistry that occurs in this complete mechanism is complex, and includes interesting aspects of C_2 chemistry, Fennimore NO_x, Cyanide chemistry, and Dark Zone chemistry common of nitro and nitramine propellants. Flame speed data was not obtained, but ignition delay and temporal flame data was.

It is important to make note of the fact that the ideal gas equation of state was used throughout the entirety of the reported Chemkin data. Real gas equations of state were explored, but showed prohibitive computational cost and high sensitivity to results. The supercritical state of the initial species does warrant the use of real gas equations of state, and this should be examined further in future research. The equations of state explored in this research were the Peng-Robinson[73] and Soave-Redlich-Kwong[74][75][76][77] equations. Though very useful for supercritical and near-supercritical fluids, these equations of state are known to have shortcomings for non-spherical and polar molecules, both of which define nitromethane and its analogs. Critical properties of all species could not be attained, and group-contribution methods cannot be used reasonably on many of these species, particularly radicals. Further work in DFT and ab-initio methods on all the species present in the mechanism could ultimately define all necessary parameters, and this, in combination with a proper equation of state for non-detonating, supercritical, polar molecules would give a more accurate answer and could be used to calculate laminar flame speed data.

Contrary to prior research by Derk,[24] soot was not seen to be present in appreciable amounts in this data. The soot mechanism used was optimized for low pressures, which is a potential source of error.[65][66] Recalculation with a

high-pressure soot mechanism, such as the TNT mechanism of Pitz and Westbook,[37] would offer a more accurate solution, however, its unlikely that soot would then show up in appreciable amounts. The soot precursor fraction is still low, and the soot calculation method of using the flame species output as the soot speciation input proved robust in that soot precursor fraction was calculated with a mechanism that has been proven at higher pressures, and soot cannot appreciate in higher quantity than the precursor content can be converted to. The observed soot described by Derk is likely the presence of a chemiluminescent species that was not predicted by the initial combustion mechanism, and possibly not even defined by the current and proposed mechanism.

The reason for the onset of this high-pressure supercrititcal initiation mechanism is speculated in this paper, though future work should focus on validating this postulate. It is the authors belief that at the supercritical temperatures and pressures in question, the compression of the carbon-nitrogen bond in nitromethane becomes stronger, while the carbon-hydrogen and nitrogen-oxygen bonds become subsequently weaker. At a certain point, carbon-nitrogen bond dissociation becomes no longer thermodynamically favorable, and its statistical probability of occurring drops as the probability of the other two bonds dissociating fully increases, leading to a shift in initiation. Typical DFT and ab-initio methods will have difficulty capturing this phenomenon.[42] Even though they can capture density and pressure effects very accurately, these methods generally don't capture temperature at all since the molecule is at a standstill, calculated at a frozen point in time. Molecular dynamics simulations

run with ab-initio or DFT methods in place of a force-field should be able to capture temperature effects, and give insight into this speculation.

References

1. Boyer, J. E., (2005) Combustion Characteristics and Flame Structure of Nitromethane Liquid Monopropellant. *Dissertation in Mechanical Engineering, The Pennsylvania State University*
2. C. Melius. Thermochemistry and Reaction Mechanisms of Nitromethane Ignition. Journal de Physique IV Colloque, 1995, 05 (C4), pp.C4-535-C4-548.
3. "Top Fuel by the Numbers". MotorTrend Magazine. TEN: The Enthusiast Network. February 2005.
4. Raviteja, S., Ramakrishna, P. A., and Ramesh, A. (November 19, 2018). "Laminar Burning Speeds of Nitromethane-Gasoline Blends at Elevated Temperatures and Pressures." ASME. J. Energy Resour. Technol. April 2019; 141(4): 042202. https://doi.org/10.1115/1.4041725
5. Heywood, John B., 1988. Internal Combustion Engine Fundamentals. McGraw-Hill Series in Mechanical Engineering, Whole Book.
6. Starkman, E., 1954. "Nitromethane as a Piston Engine Fuel" SAE Technical Paper 540186, 1954, https://doi.org/10.4271/540186.
7. S. Gordon and B. J. McBride, "Computer Program for Calculation of Complex Chemical Equilibrium Compositions and Applications," NASA Reference Publication 1311 (1996).
8. “Properties of Fuels”. WalshCarLines Fuel Properties Data Table, https://walshcarlines.com/pdf/fueltable.pdf

9. Nitromethane Technical Data Sheet, ANGUS Life Sciences Chemical Company. PDF
10. Sutton, George P., Rocket Propulsion Elements, John Wiley & Sons, New York, 1949, ch. 7.
11. Clark, John D., 1972. Ignition! An Information History of Liquid Rocket Propellants. Rutgers University Press, New Brunswick, New Jersey.
12. Morrison, W., Knapton, J. D., and Bulman, M. J., 1987. Liquid Propellant Guns. US Army Ballistic Research Laboratory, Aberdeen Proving Ground, Maryland, BRL-TR-2853.
13. Eichorn, Edgar, 1966. “The Wizardry of Propulsion”, Speer Manual for Reloading Ammunition, Number 07, *Glenn Printing Company, Kansas City, Missouri,* pp.84-96
14. Jolie, E. W., 1978. A Brief History of U.S. Navy Torpedo Development. *Naval Undersea Systems Center, Newport RI,* pp.1-150
15. Heywood, John B., and Kromer, Matthew A., 2007. Electric Powertrains: Opportunities and Challenges in the US Light-Duty Vehicle Fleet. Sloan Automotive Laboratory, Massachusetts Institute of Technology, Publication No. LFEE 2007-03 RP, All.
16. WE Bachmann, JC Sheehan (1949). "A New Method of Preparing the High Explosive RDX1". Journal of the American Chemical Society, 1949 (5):1842–1845.
17. Dinitramide Salts: ADN Plus Other Salts. SRI International, Chemical Science and Technology Laboratory, 2012

18. Varghese, T. L., and Krishnamurthy, V. N., 2017. The Chemistry and Technology of Solid Rocket Propellants (A Treatise on Solid Propellants), *Allied Publishers Pvt. Ltd. Chapter 2, Composite Propellants,* pp.20-55
19. Ricci PP, Rossi AS, Gregory OJ. Orthogonal Sensors for the Trace Detection of Explosives. IEEE Sensors Letters, 2019; 3(10), 1-4. doi: 10.1109/LSENS.2019.2944587
20. Pearson, G. S., 1968. Perchlorates: A Review of Their Thermal Decomposition and Combustion, With an Appendix on Perchloric Acid. *Rocket Propulsion Establishment, Westcott,* RPE TR No. 68/11.
21. Booth, J. S., Dollimore, D., and Heal, G. R., 1980. Thermal Analysis of Some Group I Permanganate Decompositions. *Thermochimica Acta 39(3),* pp.281-291
22. W T Borden, 2017. Why Are Addition Reactions to N2 Thermodynamically Unfavorable? *J. Phys. Chem. A.*, 121, 1140
23. Harlow, D. G., Felt, R. E., Agnew, S., Barney, G. S., McKibben, J. M., Garber, R., Lewis, M., 1998. Technical Report on Hydroxylamine Nitrate. *Department of Energy Technical Report, DOE/EH-0555.*
24. Derk, G., (2019) High Pressure Burning Rates of JA2 and Nitromethane Propellants. *Thesis in Mechanical Engineering, The Pennsylvania State University*
25. Graefe, A. F., Meyer, R. E., Mueller, K. H., (1954) Investigation of Liquid Rocket Propellants. *Aerojet-General Corporation Quarterly Report, 1-14*
26. Taylor, H. A., Vesselovsky, V. V., (1934) The Thermal Decomposition of Nitromethane. *Physical Chemistry 39, 1095-1101*

27. Cotrell, T. L., Graham, T. E., Reid, T. J., (1951) The Thermal Decomposition of Nitromethane. *Transactions of the Faraday Society 47, 584-590*
28. Mueller, K. H., (1955) The Thermal Decomposition of Nitromethane at High Pressures. *Journal of the American Chemical Society 77, 3459-3462*
29. Makovky, A., Greunwald, T. B., (1958) The Thermal Decomposition of Nitromethane Under High Pressure. *Transactions of the Faraday Society 55, 952-958*
30. Glarborg, P., Bendtsen, A. B., Miller, J. A (1999) Nitromethane Dissociation: Implications for the $CH_3 + NO_2$ Reaction. *International Journal of Chemical Kinetics Volume 35, Issue 9*; 591-602.
31. Yetter, R. A., Dryer, F. L., Allen, M. T., Gatto, J. L., (1995) Development of Gas-Phase Reaction Mechanisms for Nitramine Combustion. *Journal of Propulsion and Power 11, 683-697*
32. Han, S., van Duin, A. C. T., Goddard, W. A. (III), Strachan, A., (2011) Thermal Decomposition of Condensed-Phase Nitromethane from Molecular Dynamics from ReaxFF Reactive Dynamics. *Journal of Physical Chemistry 115, 6534-6540*
33. Rom, N., Zybin, S. V., van Duin, A. C. T., Goddard, W. A. (III), Zeiri, Y., Katz, G., Kosloff, R., (2011) Density-Dependent Liquid Nitromethane Decomposition: Molecular Dynamics Simulations Based on ReaxFF. *Journal of Physical Chemistry 115, 10181-10202*
34. Shaw, R., Decarli, P. S., Ross, D. S., Lee, E. L., Stromberg, H. D., (1979) Thermal explosion times of nitromethane, perdeuteronitromethane, and

six dinitroalkanes as a function of temperature at static high pressures of 1–50 kbar. *Combustion and Flame 35, 237-247*

35. Anderson, W. R., Meagher, N. E., Vanderhoff, J. A., (2011) Dark Zones of Solid Propellant Flames. *Army Research Laboratory, Aberdeen Proving Ground, MD 21005. Technical Report ARL -TR-5424*
36. Anderson, W. R., McQuaid, M. J., Nusca, M. J., Kotlar, A. J., (2010) A Detailed, Finite-Rate, Chemical Kinetics Mechanism for Monomethylhydrazine-Red Fuming Nitric Acid Systems. *Army Research Laboratory, Aberdeen Proving Ground, MD 21005. Technical Report ARL-TR-5088*
37. Pitz, W. J., Westbrook, C. K.. (2007) A Detailed Chemical Kinetic Model for Gas Phase Combustion of TNT. *Proceedings of the Combustion Institute 31, 2343-2351*
38. Neese, F. (2012) The ORCA program system, Wiley Interdiscip. Rev.: Comput. Mol. Sci., 2, 73-78.
39. Neese, F. (2017) Software update: the ORCA program system, version 4.0, Wiley Interdiscip. Rev.: Comput. Mol. Sci., 8, e1327.
40. Hartree, D. R. (1928). "The Wave Mechanics of an Atom with a Non-Coulomb Central Field". Math. Proc. Camb. Philos. Soc. 24 (1): 111. doi:10.1017/S0305004100011920.
41. Atkins, Peter, et. al. 2010. Shriver & Atkins' Inorganic Chemistry. *W. H. Freeman and Company, New York, NY,* Chapter Two, Molecular Structure and Bonding, pp.34-65

42. Payne, M. C., Teter, M. P., Allan, D. C., Arias, T. A., and Jounnopoulos, J. D, 1992. Iterative Minimization Techniques for Ab-Initio Total-Energy Calculations: Molecular Dynamics and Conjugate Gradients. Reviews of Modern Physics 64(4), pp.1046-1096.

43. Sherril, C. David. Basis Sets in Quantum Chemistry. *School of Chemistry and Biochemistry, Georgia Institute of Technology,* Lecture Notes.

44. X. Gonze, J.-M. Beuken, R. Caracas, F. Detraux, M. Fuchs, G.-M. Rignanese, L. Sindic, M. Verstraete, G. Zerah, F. Jollet, M. Torrent, A. Roy, M. Mikami, Ph. Ghosez, J.-Y. Raty, D.C. Allan First-principles computation of material properties: The ABINIT software project *Computational Materials Science* 25, 478-492 (2002)

45. Senftle, T., Hong, S., Islam, M. *et al.* The ReaxFF reactive force-field: development, applications and future directions. *npj Comput Mater* **2,** 15011 (2016).

46. van Duin, Adri, 2002. ReaxFF User Manual. *California Institute of Technology, Beckman Institute*

47. Strachan, Alejandro, Kober, Edward M., van Duin, Adri C. T., Oxgaard, Jonas, and Goddard, William A., 2005. Thermal Decomposition of RDX from Reactive Molecular Dynamics. *The Journal of Chemical Physics,* 122(5), 054502

48. S. Plimpton, Fast Parallel Algorithms for Short-Range Molecular Dynamics, J Comp Phys, 117, 1-19 (1995). https://lammps.sandia.gov

49. H. M. Aktulga, J. C. Fogarty, S. A. Pandit, A. Y. Grama, 2012. Parallel reactive molecular dynamics: Numerical methods and algorithmic techniques, *Parallel Computing*, 38, pp.245-259

50. Zhou, T., Liu, L., Goddard, W. III., Zybin, S., and Huang, F., 2014. ReaxFF Reactive Molecular Dynamics on Silicon Pentaerythritol Tetranitrate Crystal Validates the Mechanism for the Colossal Sensitivity. *Journal of Physical Chemistry and Chemical Physics,* 43(16), pp.23779-23791

51. Lianchi Liu, Yi Liu, Sergey V. Zybin, Huai Sun, and William A. Goddard, 2011. ReaxFF-lg: Correction of the ReaxFF Reactive Force Field for London Dispersion, with Applications to the Equations of State for Energetic Materials *The Journal of Physical Chemistry A 2011 115 (40),* 11016-11022 DOI: 10.1021/jp201599t

52. Walker, F. E., 1979. Initiation and Detonation Studies in Sensitized Nitromethane. *Acta Astronautica, 6(7-8),* pp.807-813

53. Yuri A. Gruzdkov and Yogendra M. Gupta, 1998. Mechanism of Amine Sensitization in Shocked Nitromethane, *The Journal of Physical Chemistry A 1998 102 (13),* 2322-2331 DOI: 10.1021/jp9803236

54. Dattelbaum, D & Sheffield, S & Bartram, Brian & Gibson, L & Bowden, Patrick & Schilling, B. (2014). The shock sensitivities of nitromethane/methanol mixtures. *Journal of Physics: Conference Series. 500. 182009. 10.1088/1742-6596/500/18/182009.*

55. Zeman, S. et al. 2009. Accounts of New Aspects of Nitromethane Sensitivity. *Central European Journal of Energetic Materials*, 2009, 6(1), 119-133.

56. Wendler, K., Thar, J., Zahn, S. and Kirchner, B., 2010. Estimating the Hydrogen Bond Energy. The Journal of Physical Chemistry A, 114(35), pp.9529-9536.
57. Kwan, E., 2009. Introduction To Hydrogen Bonding.
58. Gregory P. Smith, David M. Golden, Michael Frenklach, Nigel W. Moriarty, Boris Eiteneer, Mikhail Goldenberg, C. Thomas Bowman, Ronald K. Hanson, Soonho Song, William C. Gardiner, Jr., Vitali V. Lissianski, and Zhiwei Qin, *GRIMech 3.0 Chemical Kinetic Mechanism,* http://www.me.berkeley.edu/gri_mech/
59. Lindemann, F. A., 1922. Transactions of the Faraday Society Volume 17, p.598
60. Christiansen, J. A., 1922 International Journal of Research in Physical Chemistry and Chemical Physics, 103 pp.91-98
61. Peters, Baron. 2017. Unimolecular Reactions. Reaction Rate Theory and Rate Events Simulations, pp.209-225
62. Marcus, R. A. 1952. Unimolecular Dissociations and Free Radical Recombination Reactions. The Journal of Chemical Physics, 20(3) pp.359-364
63. CHEMKIN-PRO 15112, User Manual Reaction Design: San Diego, 2011
64. Luo, Yu-Ran. 2009. Bond Dissociation Energies. CRC BDE Tables 9 pp. 65-98.
65. Ali Ergut, Silvia Granata, Jude Jordan, Joel Carlson, Jack B. Howard, Henning Richter and Yiannis A. Levendis. 2006. PAH Formation in One-

Dimensional Premixed Fuel-Rich Atmospheric Pressure Ethylbenzene and Ethyl-Alcohol Flames. *Combustion and Flame*

66. Richter, H., et al. 2005. Detailed modeling of PAH and soot formation in a laminar premixed benzene/oxygen/argon low-pressure flame. *Proceedings of the Combustion Institute, 30(1),* pp. 1397-1405
67. Blanquart, G., Pepiot-Desjardians, and P., Pitsch, H., 2009. Chemical Mechanism for High Temperature Combustion of Engine Relevant Fuels with Emphasis on Soot Precursors. Combustion and Flame, 156, pp.588-607
68. Takahashi, F., and Glassman, I., 1984. Sooting Correlations for Premixed Flames. Combustion Science and Technology, 37(1-2) pp.1-19
69. CHEMKIN-PRO 15112, Reaction Design: San Diego, 2011
70. Gardiner, W. C. Jr., Dean, A. M., and Bozzelli, J. W., 2000. Combustion Chemistry of Nitrogen. Gas Phase Combustion Chemistry, Springer Science and Business Media, pp.125-316.
71. Fenimore, C P (1971). "Formation of nitric oxide in premixed hydrocarbon flames". Symposium (International) on Combustion. 13 (1): 373–380. doi:10.1016/S0082-0784(71)80040-1.
72. Y.B. Zel'dovich (1946). "The Oxidation of Nitrogen in Combustion Explosions". Acta Physicochimica U.S.S.R. 21: 577–628.
73. Peng, D. Y.; Robinson, D. B. (1976). "A New Two-Constant Equation of State". Industrial and Engineering Chemistry: Fundamentals. 15: 59–64. doi:10.1021/i160057a011.

74. Redlich, Otto.; Kwong, J. N. S. (1949-02-01). "On the Thermodynamics of Solutions. V. An Equation of State. Fugacities of Gaseous Solutions". Chemical Reviews. 44 (1): 233–244. doi:10.1021/cr60137a013. ISSN 0009-2665. PMID 18125401.
75. Soave, Giorgio (1972). "Equilibrium constants from a modified Redlich-Kwong equation of state". Chemical Engineering Science. 27 (6): 1197–1203. doi:10.1016/0009-2509(72)80096-4.
76. Soave, Giorgio (1972). "Equilibrium constants from a modified Redlich-Kwong equation of state". Chemical Engineering Science. 27 (6): 1197–1203. doi:10.1016/0009-2509(72)80096-4.
77. Peneloux, A.; Rauzy, E.; Freze, R. (1982). "A Consistent Correction for Redlich-Kwong-Soave Volumes". Fluid Phase Equilibria. 8 (1982): 7–23. doi:10.1016/0378-3812(82)80002-2.
78. Soave, G.; Fermeglia, M. (1990). "On the Application of Cubic Equation of State to Synthetic High-Pressure VLE Measurements". Fluid Phase Equilibria. 60 (1990): 261–271. doi:10.1016/0378-3812(90)85056-G.

Appendix A: Full Reaction Set in Chemkin Format

*Activation Energy is in calories/mole, default units for Chemkin

REACTIONS	A	b	Ea
CH3NO2 = CH2NO2 + H	6.50E04	0.00	10000
CH3NO2 = CH3NO + O	1.40E04	0.00	3730
CH3NO2 + H = CH3NOOH	4.42E04	2.64	4042
CH3NOOH = CH3NO + OH	7.50E04	0.00	3730
CH3NOOH = CH3NOH + OH	7.50E04	0.00	3730
CH3NOOH = CH3O + HNO	1.00E13	0.00	36000
CH3NOOH = CH3 + HONO	1.78E16	0.00	58490
CH3NOH = CH3 + HNO	1.78E16	0.00	58490
CH3NO + M = H2CNOH + M	1.50E13	0.00	500
CH3NO = CH3 + NO	1.78E16	0.00	58490
H2CNOH + M = H2CNO + H + M	1.60E16	0.00	86360
CH2NO2 + H = CH2NOOH	4.42E04	2.64	4042
CH2NOOH = OH + H2CNO	7.50E04	0.00	3730
CH2NOOH = CH2 + HONO	1.78E16	0.00	58490
CH2NOOH = CH2O + HNO	1.00E13	0.00	36000
CH3NO2 + H2O => CH3NO + H2O2	1.40E04	0.00	3730
CH3NO2 + H2O2 => CH2NOOH + HO2 + H	3.30E12	0.00	3730
CH3NO + HO2 => H2CNO + H2O2	1.70E04	2.48	-2420
CH2NO2 + OH => H2CNO + H + O2	3.30E12	0.00	3730
CH3NO2 + M => H2CNO + OH + M	3.30E12	0.00	66000
CH3NO2 + OH => H + H + O2 + H2CNO	3.30E12	0.00	89360

END

Appendix B: Output Log Sample

```
# Timestep    No_Moles    No_Specs    CH3O2N
69      125       1       125
# Timestep    No_Moles    No_Specs    CH3O2N
119     125       1       125
# Timestep    No_Moles    No_Specs    CH3O2N
169     125       1       125
# Timestep    No_Moles    No_Specs    CH3O2N    CH2O2N      H
219     127       3       123     2       2
# Timestep    No_Moles    No_Specs    CH3O2N    CH2O2N      H
269     134       3       116     9       9
# Timestep    No_Moles    No_Specs    CH3O2N    CH2O2N      H
319     143       3       107     18      18
# Timestep    No_Moles    No_Specs    CH3O2N    CH2O2N      H
369     157       3       93      32      32
# Timestep    No_Moles    No_Specs    CH3O2N    CH2O2N      H
419     172       3       78      47      47
# Timestep    No_Moles    No_Specs    CH3O2N    CH2O2N      H
469     181       3       69      56      56
# Timestep    No_Moles    No_Specs    CH3O2N    CH2O2N      H
519     192       3       58      67      67
# Timestep    No_Moles    No_Specs    CH3O2N    CH2O2N      H
569     202       3       48      77      77
# Timestep    No_Moles    No_Specs    CH3O2N    CH2O2N      H
619     209       3       41      84      84
# Timestep    No_Moles    No_Specs    CH2O2N    H       CH3O2N
669     218       3       93      93      32
# Timestep    No_Moles    No_Specs    CH2O2N    H       CH3O2N
719     220       3       95      95      30
# Timestep    No_Moles    No_Specs    CH2O2N    H       CH3O2N      CH4O2N
769     220       4       96      95      28      1
# Timestep    No_Moles    No_Specs    CH2O2N    H       CH3O2N      CH4O2N
819     221       4       97      96      27      1
# Timestep    No_Moles    No_Specs    CH2O2N    H       CH3O2N      CH4O2N
```

869 223 4 99 98 25 1

Timestep No_Moles No_Specs CH2O2N H CH3O2N CH4O2N

919 224 4 100 99 24 1

Timestep No_Moles No_Specs CH2O2N H CH3O2N CH4O2N

969 226 4 102 101 22 1

Timestep No_Moles No_Specs CH2O2N H CH3O2N CH4O2N

1019 227 4 103 102 21 1

Timestep No_Moles No_Specs CH2O2N H CH3O2N CH4O2N

1069 227 4 103 102 21 1

Timestep No_Moles No_Specs CH2O2N H CH3O2N CH4O2N

1119 226 4 102 101 22 1

Timestep No_Moles No_Specs CH2O2N H CH3O2N CH4O2N

1169 226 4 102 101 22 1

Timestep No_Moles No_Specs CH2O2N H CH3O2N CH4O2N

1219 226 4 102 101 22 1

Timestep No_Moles No_Specs CH2O2N H CH4O2N CH3O2N

1269 225 4 102 100 2 21

Timestep No_Moles No_Specs CH2O2N H CH4O2N CH3O2N

1319 224 4 101 99 2 22

Timestep No_Moles No_Specs CH2O2N H CH4O2N CH3O2N

1369 225 4 102 100 2 21

Timestep No_Moles No_Specs CH2O2N H CH4O2N CH3O2N

1419 225 4 102 100 2 21

Timestep No_Moles No_Specs CH2O2N H CH4O2N CH3O2N C2H6O4N2

1469 224 5 102 100 2 19 1

Timestep No_Moles No_Specs CH2O2N H CH4O2N CH3O2N

1519 224 4 101 99 2 22

Timestep No_Moles No_Specs CH2O2N H CH4O2N CH3O2N

1569 224 4 101 99 2 22

Timestep No_Moles No_Specs CH2O2N H CH3O2N CH4O2N

1619 223 4 100 98 23 2

Timestep No_Moles No_Specs CH2O2N H CH3O2N CH4O2N

1669 222 4 99 97 24 2

Timestep No_Moles No_Specs CH2O2N H CH3O2N CH4O2N
1719 223 4 100 98 23 2
Timestep No_Moles No_Specs CH2O2N H CH3O2N CH4O2N
1769 223 4 100 98 23 2
Timestep No_Moles No_Specs CH2O2N H CH3O2N CH4O2N
1819 223 4 100 98 23 2
Timestep No_Moles No_Specs CH2O2N H CH3O2N C2H6O4N2 CH4O2N
1869 222 5 100 98 21 1 2
Timestep No_Moles No_Specs CH2O2N H CH3O2N CH4O2N
1919 222 4 99 97 24 2
Timestep No_Moles No_Specs CH2O2N H CH3O2N CH4O2N
1969 222 4 99 97 24 2
Timestep No_Moles No_Specs CH2O2N H CH3O2N CH4O2N
2019 222 4 99 97 24 2
Timestep No_Moles No_Specs CH2O2N H CH3O2N CH4O2N
2069 222 4 99 97 24 2
Timestep No_Moles No_Specs CH2O2N H CH3O2N CH4O2N
2119 223 4 100 98 23 2
Timestep No_Moles No_Specs CH2O2N H CH3O2N CH4O2N
2169 223 4 101 98 21 3
Timestep No_Moles No_Specs CH2O2N H CH3O2N CH4O2N
2219 223 4 101 98 21 3
Timestep No_Moles No_Specs CH2O2N H CH3O2N CH4O2N
2269 224 4 102 99 20 3
Timestep No_Moles No_Specs CH2O2N H CH3O2N CH4O2N
2319 223 4 101 98 21 3
Timestep No_Moles No_Specs CH2O2N H CH3O2N CH4O2N
2369 223 4 101 98 21 3
Timestep No_Moles No_Specs CH2O2N H CH3O2N CH4O2N
2419 223 4 101 98 21 3
Timestep No_Moles No_Specs CH2O2N H CH3O2N CH4O2N
2469 223 4 101 98 21 3
Timestep No_Moles No_Specs CH2O2N H CH3O2N CH4O2N

2519 222 4 100 97 22 3

Timestep No_Moles No_Specs CH2O2N H CH3O2N CH4O2N

2569 222 4 100 97 22 3

Timestep No_Moles No_Specs CH2O2N H CH3O2N CH4O2N

2619 222 4 100 97 22 3

Timestep No_Moles No_Specs CH2O2N H CH3O2N CH4O2N

2669 222 4 100 97 22 3

Timestep No_Moles No_Specs CH2O2N H CH3O2N CH4O2N

2719 222 4 100 97 22 3

Timestep No_Moles No_Specs CH2O2N H CH3O2N CH4O2N

2769 222 4 100 97 22 3

Timestep No_Moles No_Specs CH2O2N H CH3O2N CH4O2N

2819 223 4 101 98 21 3

Timestep No_Moles No_Specs CH2O2N H CH3O2N CH4O2N

2869 224 4 101 99 22 2

Timestep No_Moles No_Specs CH2O2N H CH3O2N CH4O2N

2919 224 4 101 99 22 2

Timestep No_Moles No_Specs CH2O2N H CH3O2N CH4O2N

2969 224 4 101 99 22 2

Timestep No_Moles No_Specs CH2O2N H CH3O2N CH4O2N

3019 224 4 101 99 22 2

Timestep No_Moles No_Specs CH2O2N H CH3O2N CH4O2N

3069 225 4 102 100 21 2

Timestep No_Moles No_Specs CH2O2N H CH3O2N CH4O2N

3119 225 4 102 100 21 2

Timestep No_Moles No_Specs CH2O2N H CH3O2N CH4O2N

3169 225 4 102 100 21 2

Timestep No_Moles No_Specs CH2O2N H CH3O2N CH4O2N

3219 225 4 102 100 21 2

Timestep No_Moles No_Specs CH2O2N H CH3O2N CH4O2N

3269 225 4 102 100 21 2

Timestep No_Moles No_Specs CH2O2N H CH3O2N CH4O2N

3319 225 4 102 100 21 2

Timestep No_Moles No_Specs CH2O2N H CH3O2N CH4O2N

Appendix C: LAMMPS Input Sample

LAMMPS (12 Dec 2018)

```
units           real

atom_style      charge
read_data       NitroMeth.data

replicate       5 5 5
pair_style      reax/c lmp_control
pair_coeff      * * ffield.reax.rdx C H N O

neighbor        2 bin
neigh_modify    every 10 delay 0 check no


fix     1 all npt temp 800.0 800.0 1.0 iso 2380 2380 10.0
fix     2 all qeq/reax 1 0.0 10.0 1e-6 param.qeq


thermo          100
compute         reax all pair reax/c
variable        eb equal c_reax[1]
variable        ea equal c_reax[2]
variable        elp equal c_reax[3]
variable        emol equal c_reax[4]
variable        ev equal c_reax[5]
variable        epen equal c_reax[6]
variable        ecoa equal c_reax[7]
variable        ehb equal c_reax[8]
variable        et equal c_reax[9]
```

```
variable        eco equal c_reax[10]
variable        ew equal c_reax[11]
variable        ep equal c_reax[12]
variable        efi equal c_reax[13]
variable        eqeq equal c_reax[14]
thermo_style custom step temp press density epair v_eb v_ea v_elp v_emol
v_ev v_epen v_ecoa v_ehb v_et v_eco v_ew v_ep v_efi v_eqeq
thermo_modify   lost warn


min_style       cg
minimize        1e-10 1e-10 5000 10000

velocity        all create 800 4759206834 dist gaussian

fix     4 all reax/c/species 5 10 50 species.out
fix     3 all reax/c/bonds 500 bonds.out
timestep    0.01
run         500
unfix       1
fix         1 all nph iso 2380 2380 5.0
timestep    0.05
run         200000
```

Appendix D: Nitromethane XYZ File Sample

LAMMPS data file written by OVITO

7 atoms
4 atom types

-8 -1.5 xlo xhi
-1 5 ylo yhi
-1 2.14 zlo zhi

Masses

1	12.0107
2	1.00794
4	14.0067
3	15.9994

Atoms

1	1	0.0	-7.1718998	3.54931	-0.07865
2	4	1.0	-5.6966801	3.52367	0.1097
3	2	0.0	-7.3603301	3.80617	-1.1228
4	2	0.0	-7.5843702	4.3026199	0.59587
5	2	0.0	-7.5730901	2.5620899	0.16042
6	3	-1.0	-5.1244602	4.6171899	0.1899
7	3	0.0	-5.1517801	2.4144101	0.15335

*Vary xlo, ylo, zlo, xhi, yhi, and zhi to achieve different initial densities for the LAMMPS Simulation